

UNCLASSIFIED

AD **298 278**

*Reproduced
by the*

ARMED SERVICES TECHNICAL INFORMATION AGENCY
ARLINGTON HALL STATION
ARLINGTON 12, VIRGINIA



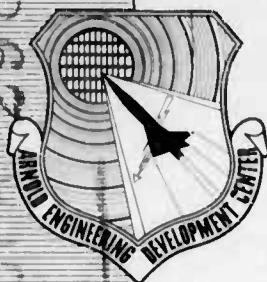
UNCLASSIFIED

NOTICE: When government or other drawings, specifications or other data are used for any purpose other than in connection with a definitely related government procurement operation, the U. S. Government thereby incurs no responsibility, nor any obligation whatsoever; and the fact that the Government may have formulated, furnished, or in any way supplied the said drawings, specifications, or other data is not to be regarded by implication or otherwise as in any manner licensing the holder or any other person or corporation, or conveying any rights or permission to manufacture, use or sell any patented invention that may in any way be related thereto.

63 2-6

AEDC-TDR-63-35

298278



VISCOUS EFFECTS ON ZERO-LIFT DRAG OF SLENDER BLUNT CONES

By

Jack D. Whitfield and B. J. Griffith
von Kármán Gas Dynamics Facility
ARO, Inc.

TECHNICAL DOCUMENTARY REPORT NO. AEDC-TDR-63-35

March 1963

MAR 18 1963

AFSC Program Area 806A, Project 8951, Task 895103

(Prepared under Contract No. AF 40(600)-1000 by ARO, Inc.,
contract operator of AEDC, Arnold Air Force Station, Tenn.)

298 278

**ARNOLD ENGINEERING DEVELOPMENT CENTER
AIR FORCE SYSTEMS COMMAND
UNITED STATES AIR FORCE**

NOTICES

Qualified requesters may obtain copies of this report from ASTIA. Orders will be expedited if placed through the librarian or other staff member designated to request and receive documents from ASTIA.

When Government drawings, specifications or other data are used for any purpose other than in connection with a definitely related Government procurement operation, the United States Government thereby incurs no responsibility nor any obligation whatsoever; and the fact that the Government may have formulated, furnished, or in any way supplied the said drawings, specifications, or other data, is not to be regarded by implication or otherwise as in any manner licensing the holder or any other person or corporation, or conveying any rights or permission to manufacture, use, or sell any patented invention that may in any way be related thereto.

VISCOUS EFFECTS ON ZERO-LIFT DRAG
OF SLENDER BLUNT CONES

By

Jack D. Whitfield and B. J. Griffith
von Kármán Gas Dynamics Facility

ARO, Inc.

a subsidiary of Sverdrup and Parcel, Inc.

March 1963

ARO Project No. VT2149

FOREWORD

The authors wish to acknowledge contributions to this research work by many of their colleagues at the von Kármán Gas Dynamics Facility, Arnold Engineering Development Center. Among the many who assisted in this work, the following specific contributors are noted:

C. H. Lewis for his assistance with the similar solutions, J. Leith Potter and his staff for their assistance in obtaining the low-density hypervelocity drag data, and H. T. Wood, Jr. and his staff for their assistance in obtaining the Mach 10 continuum drag data.

The authors are grateful to K. D. Bird and his staff at the Cornell Aeronautical Laboratory for their efforts in obtaining the Shock-Tunnel cone drag data used herein.


ABSTRACT

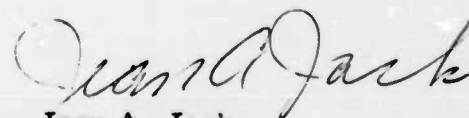
Experimental drag data from a series of cone models are presented over a wide range of Reynolds numbers at hypersonic flow conditions. The data include Mach numbers from 9 to 22 with Reynolds numbers based on model length ranging from 600 to 500,000. Most data were obtained with test model surface temperature cold relative to the stagnation temperature; a limited amount of hot-wall data were obtained.

Theoretical estimates based on existing theories are given, and the significant contributions to the zero-lift, viscous drag rise of cold-wall cones are identified as the usual "similar" or Blasius friction drag and transverse curvature effects. The theoretical estimates are shown to offer a good engineering approximation to the hypersonic viscous drag of cold-wall, blunt slender cones within the continuum flow regime.

PUBLICATION REVIEW

This report has been reviewed and publication is approved.


Donald R. Eastman, Jr.
DCS/Research


Jean A. Jack
Colonel, USAF
DCS/Test

CONTENTS

	<u>Page</u>
ABSTRACT.	v
NOMENCLATURE.	ix
1.0 INTRODUCTION	1
2.0 TEST APPARATUS	
2.1 Wind Tunnels.	1
2.2 Models and Instrumentation	3
3.0 PRECISION OF MEASUREMENTS	
3.1 Hypervelocity Data	3
3.2 Low-Density Hypervelocity Data	5
3.3 50-Inch Mach 10 Tunnel (C) Data	5
4.0 THEORETICAL CONSIDERATIONS	
4.1 Similar Solutions	6
4.2 Viscous Interaction Effects	7
4.3 Total Zero-Lift Drag Estimate.	12
5.0 EXPERIMENTAL RESULTS	13
6.0 CONCLUDING REMARKS	15
REFERENCES	16
APPENDIX I: TABULATED ZERO-LIFT DRAG DATA	19

TABLES

1. VKF Cone Drag Models	23
2. Results from Similar Solutions	23

ILLUSTRATIONS

Figure

1. The 16-Inch Hypervelocity Tunnel (Hotshot 1)	24
2. The 50-Inch Hypervelocity Tunnel (Hotshot 2)	25
3. Low-Density Hypervelocity Wind Tunnel.	26
4. The 50-Inch Mach 10 Tunnel (C)	28
5. Cone Nomenclature	29
6. Photograph of Cone Drag Models	30

<u>Figure</u>		<u>Page</u>
7.	Cone Pressure Distributions for Bluntness Ratios ≥ 0.3	31
8.	Assumed and Actual Cone Pressure Distributions for Bluntness Ratios ≤ 0.03	31
9.	Theoretical Drag Components for 9-deg Half-Vertex Angle Blunt Cone	32
10.	Comparison of Theory and Experiment in Continuum Flow Regime, 6.34-deg Half-Vertex Angle Cones	33
11.	Comparison of Theory and Experiment in Continuum Flow Regime, 9-deg Half-Vertex Angle Cones	34
12.	Comparison of Theory and Experiment in Continuum Flow Regime, 13.5-deg Half-Vertex Angle Cone	35
13.	Comparison of Hypersonic, Cold Wall, Viscous Drag of Blunt, Slender Cones in Continuum and Rarefied Flow Regimes	36

NOMENCLATURE

A	Constant obtained by Cohen and Reshotko integral method (see Eq. 2)
a	Local speed of sound
B	Proportionality constant (see Eq. 5)
C_e	Form of Chapman-Rubesin viscosity coefficient, $(\mu_w/\mu_e) (T_e/T_w)$
C_∞	Form of Chapman-Rubesin viscosity coefficient, $(\mu_w/\mu_\infty) (T_\infty/T_w)$
C_D	Total forebody drag coefficient based on base area (see Eq. 11)
C_{DN}	Inviscid model nose drag coefficient
C_{D0}	Inviscid pressure drag coefficient based on base area
\bar{C}_{Df}	Average skin-friction coefficient based on similar solutions, $(\int_S \bar{\tau}_w dS_w)/q_\infty S_B$
$(\Delta C_{Df})_p$	Incremental increase in average skin-friction coefficient caused by induced pressure (see Eq. 8)
$(\Delta C_{Df})_{tc}$	Incremental increase in average skin-friction coefficient caused by transverse curvature effects (see Eq. 10)
$(\Delta C_D)_p$	Incremental increase in pressure drag caused by induced pressure (see Eq. 4)
C_p	Pressure coefficient, $(p - p_\infty)/q_\infty$
\bar{C}_{pc}	Average inviscid pressure coefficient for conical section of body
\bar{c}_f	Local similar skin-friction coefficient, $(2 \bar{\tau}_w)/(\rho_w u_e^2)$
$(\Delta c_f)_p$	Incremental increase in local skin-friction coefficient caused by induced pressure (see Eq. 6)
$(\Delta c_f)_{tc}$	Incremental increase in local skin-friction coefficient caused by transverse curvature effects (see Eq. 9)
c_p	Specific heat at constant pressure
c_v	Specific heat at constant volume
d_B	Model base diameter

d_N	Model nose diameter
d_∞	Function of surface temperature, gas properties, and free-stream conditions (see Eq. 3, also Ref. 18)
K	Hypersonic similarity parameter, $M_\infty \theta_c$
k	Coefficient of thermal conductivity of gas
L	Overall model length
M	Mach number, u/a
$(Me)_L$	Local surface Mach number at length, L
Pr	Prandtl number, $(c_p u)/k$
p'_0	Stagnation pressure behind normal shock
Δp	Increase in pressure caused by displacement induced pressure gradient
p	Pressure
q_∞	Free-stream dynamic pressure, $1/2 \rho_\infty u_\infty^2$
Re_w	Local Reynolds number $(\rho_w u_e s)/\mu_w$
$Re_{\infty, L}$	Reynolds number based on model length, $(\rho_\infty u_\infty L)/\mu_\infty$
r	Local body radius
S_B	Model base area
S_w	Model wetted surface area
s	Distance along model surface from stagnation point
T	Temperature
u	Velocity
\bar{v}_∞	Viscous parameter, $(\sqrt{\bar{C}_\infty} M_\infty)/\sqrt{Re_{\infty, L}}$
x	Distance along model axis of symmetry from stagnation point
γ	Ratio of specific heats, c_p/c_v
δ	Boundary-layer thickness
δ^*	Boundary-layer displacement thickness
$\epsilon \equiv$	$\gamma - 1/\gamma + 1$
θ_c	Cone half-vertex angle
μ	Gas viscosity

ρ	Gas density
τ_w	Surface shear stress from similar solutions
X	Hypersonic viscous interaction parameter, $(\sqrt{C_e} M_e^3) / \sqrt{(\rho_e u_e s) / \mu_e}$
\bar{X}_L	Hypersonic viscous interaction parameter based on model length, L
ψ	Nose bluntness ratio, r_N / r_B

SUBSCRIPTS

B	Model base dimension
e	Edge of boundary-layer conditions
N	Model nose dimension
o	Total stagnation conditions
w	Model wall conditions
∞	Free-stream conditions

1.0 INTRODUCTION

The often dominant role of viscous effects on the aerodynamics of slender bodies at hypersonic speeds is now widely recognized and has been the subject of many theoretical and experimental papers. The phenomena of interactions between inviscid and viscous flow fields complicate both theoretical and experimental studies of viscous effects at hypersonic speeds.

The complexity of the combined problem demands recourse to both theory and experiment. Unfortunately, the available experimental data have usually been limited to supersonic rather than hypersonic speeds or to the more academic cases wherein the model surface temperature is near the total stagnation temperature. It is the purpose of this paper to present viscous drag data from slender blunt cones at hypersonic speeds with both hot and cold model surface temperatures relative to the total stagnation temperature. These experimental results were obtained from the hypersonic wind tunnels of the von Kármán Gas Dynamics Facility (VKF), Arnold Engineering Development Center (AEDC), Air Force Systems Command (AFSC). Preliminary results from this research were previously published in Refs. 1 and 2.

During the course of this research, considerable inviscid as well as viscous dominated data were obtained from blunt slender cones. Shock shapes and pressure distributions were published by Lewis (Ref. 3), and revisions to the pressure distributions were published by Whitfield and Norfleet (Ref. 4). Inviscid hypersonic, static stability data from blunt slender cones were published by Whitfield and Wolny (Ref. 5).

2.0 TEST APPARATUS

2.1 WIND TUNNELS

The experimental data reported herein were obtained in four of the VKF hypersonic wind tunnels:

1. The 16-Inch Hypervelocity Tunnel (Hotshot 1), (Fig. 1) (Ref. 2)
2. The 50-Inch Hypervelocity Tunnel (Hotshot 2), (Fig. 2) (Ref. 2)

Manuscript received January 1963.

3. The Low-Density Hypervelocity Tunnel, (Fig. 3) (Ref. 6)
4. The 50-Inch Mach 10 Tunnel (C), (Fig. 4) (Ref. 7)

The 16-inch and 50-inch hotshot tunnels (Figs. 1 and 2) are electric-arc-heated hypervelocity wind tunnels using nitrogen as a test gas. Conical nozzles (5-deg half-angle) were used in both hotshot tunnels. Stagnation temperatures were sufficient, even without supercooling, to avoid theoretical liquefaction of the test gas at test-section conditions. Relatively small variations in Mach number were obtained during the hotshot tests (Table 1); the primary emphasis was on variations in Reynolds number. During the relatively short run time (~ 0.05 sec) of a hotshot wind tunnel, the wall temperature of a test model does not change significantly: thus, a wall to stagnation temperature ratio of approximately 0.1 was obtained for all of the hotshot tests.

The Low-Density Hypervelocity Tunnel (Fig. 3) described by Potter, et. al. (Ref. 6) is an arc-heated, continuously operating facility with a nominal Mach number 9 nozzle. A small axial Mach number gradient, approximately 0.25 per inch, existed during the tests reported herein. All of the free-stream conditions used here are based on conditions at the model nose, and typical Mach number increases over the length of the body in the undisturbed free stream amount to approximately four percent. Nitrogen was used as a test gas, and the reservoir temperature and pressure ranged from 2000 to 3000°K and 23 to 18 psia, respectively, for these tests. Measurements of total enthalpy at the nozzle throat by calorimetry (Ref. 8) agree closely with total enthalpy computed on the basis of measured mass flow rate, total pressure, sonic throat area, and the assumption of thermodynamic equilibrium in the fluid upstream of the throat. However, on the basis that computed relaxation lengths for molecular vibration downstream from the throat are from 10^2 to 10^4 times local nozzle radius, all theoretical evidence indicates frozen flow from the throat onward. Thus, test-section flow characteristics are based on sudden freezing of the flow at the throat. Although this tunnel is capable of continuous operation, in view of the low rate of convective heat transfer and a significant radiant heat loss from the model to the relatively cool surroundings, a relatively cold model surface temperature is maintained. Model surface temperatures of approximately 600°K were estimated from optical pyrometry measurements; hence, wall to stagnation temperature ratios of 0.2 to 0.3 are assumed.

The 50-Inch Mach 10 Tunnel (C) (Fig. 4) is a continuously operating facility using air as a test gas. Air, heated to approximately 1900°R (sufficient to avoid liquefaction) by a propane-fired gas heater and an

electric-resistance heater in series, is expanded through a contoured Mach 10 nozzle. Radiant heat losses from the test model to the water-cooled nozzle walls produced an equilibrium model surface temperature less than the adiabatic value. Model surface temperature to total stagnation temperature ratios of approximately 0.65 to 0.75 were obtained. The variations in this ratio were due to changes in the convective heat-transfer rate with dynamic pressure with the radiant heat losses remaining essentially constant.

2.2 MODELS AND INSTRUMENTATION

Geometrical parameters and model sizes for the various cone drag models used in this research are tabulated in Table 1 (see Fig. 5 for nomenclature). Typical models are shown in Fig. 6. All of the models used in the hotshot tests were of a light-weight construction using fiberglass and epoxy resin. Stainless steel models were used in the Low-Density Hypervelocity Tunnel and the 50-Inch Mach 10 Tunnel (C).

Pressure and drag measurements in the hotshot tunnels were accomplished using the transducers and techniques as described in Refs. 1, 2, and 9. Measurements of pitot pressure (hence dynamic pressure) and drag were obtained simultaneously for all of the hotshot tests. Although variations in dynamic pressure were no more than ± 10 percent for repeated tunnel runs, the simultaneous measurements of pitot pressure and drag served to minimize the influence of these run-to-run variations.

Drag measurements from the quite small models in the Low-Density Hypervelocity Tunnel and the 50-Inch Mach 10 Tunnel (C) required the development of a special water-cooled balance. A sting-type axial-force balance was developed using a parallelogram flexure arrangement. The deflection-sensing element was a differential transformer. It is worthwhile to note that a zero-lift drag level of 0.003 lb has been measured with a repeatability of ± 5 percent.

3.0 PRECISION OF MEASUREMENTS

3.1 HYPERVELOCITY DATA

The accuracy of results from any high temperature, hypervelocity test facility is, of course, a function not only of the uncertainty of the direct measurements but also of the validity of the assumptions and the

gas properties used in inferring the flow conditions. For example, it has been recently shown in Ref. 2 that the conventional method used in hotshot wind tunnels for arriving at the enthalpy of the test gas by using the measured arc-chamber pressure and an initial knowledge of the gas density may contain appreciable error. It was established in Ref. 2, by direct measurement of the flow velocity, that the measured stagnation heat rate is a suitable monitor of the total flow enthalpy. During the present tests* measured stagnation heat rates and measured pitot pressures (obtained simultaneously) were used together with Fay-Riddell stagnation point theory (Ref. 10) to compute the timewise total flow enthalpy. With the measured arc-chamber total pressure, measured test-section pitot pressure, total enthalpy from the stagnation heat rate, and the assumption of isentropic nozzle flow, all other flow parameters (e. g. Mach number, Reynolds number) may be computed directly (see Ref. 11).

Uncertainties in the measured stagnation heat rates will, of course, enter the uncertainty and spread in the experimental drag data. An estimate of the uncertainty in the viscous parameter, $\bar{v}_\infty \equiv \sqrt{C_\infty} M_\infty / \sqrt{Re_\infty} L$, used later for data presentation and correlation, may be obtained from the spread of measured heat rates. The ± 5 percent spread of flow velocities inferred from stagnation heat rates as compared to measured flow velocities (see Ref. 2) corresponds to ± 10 percent spread in the heat rate data (assuming a perfect measurement of flow velocity). A heat rate spread of ± 10 percent leads to an estimated uncertainty of ± 7 percent in the viscous parameter, and this combined with an estimated uncertainty of ± 5 percent in the drag measurements leads, for a normal distribution of random errors, to ± 8 percent spread in the correlated data. This estimated uncertainty is compatible with the data presentations where a repeatability of ± 10 percent is apparent.

Experiments with the 6.34-deg cones were the exception to the above, outlined procedure for defining free-stream conditions. During these tests, stagnation heat rates were not obtained simultaneously with the drag measurements and the pitot and arc-chamber pressure measurements; therefore, the old method of computing the total enthalpy (see Ref. 11) by assuming a uniform distribution of energy within the arc-chamber was used. Based on correlations of measured velocities and inferred velocities from the computed arc-chamber enthalpy, uncertainties of ± 13 percent are estimated for the viscous parameter. This uncertainty leads to an estimated uncertainty of ± 14 percent in the correlated drag data from the 6.34-deg cones. It is believed that these uncertainties are large; however, the lack of data prevents a more accurate assessment.

*With the exception of drag data obtained from the 6.34-deg cones, see later discussion.

All of the hotshot data presented herein were obtained with conical nozzles. The influence of the resulting source flow on the inviscid pressure distribution over slender sharp cones was studied in Ref. 4. The pressure distributions used herein for theoretical estimates were corrected for the sharper cone cases ($\psi \leq 0.03$) by the method of Ref. 4; however, no corrections were applied to the measured total drag data reported here. The total drag data will be shown later to be largely viscous dominated, and hence the influence of source flow effects on the inviscid drag outlined in Ref. 4 is not directly applicable. An experimental check on the possible magnitude of source flow effects on the drag of slender cones was accomplished by varying the model size at different stream Reynolds numbers. The resulting data from different size models (see Table 1) are in reasonable agreement in terms of the correlation parameter, $\bar{v}_\infty \equiv \sqrt{C_\infty M_\infty / \sqrt{Re_\infty L}}$. It is not meant to imply here that the source flow effects are always negligible in slender cone viscous drag data; however, it is believed that these effects are negligible in the viscous drag data presented herein.

3.2 LOW-DENSITY HYPERVELOCITY DATA

Again, as in the hotshot data, the validity of the assumptions and gas properties used in inferring the flow conditions affect the accuracy of the data. The initial calibration of the Low-Density Hypervelocity Tunnel (LDH) was discussed by Potter, et. al. (Ref. 6) and Arney and Boylan (Ref. 8). Since the calibration report by Potter, et. al. (Ref. 6), a new nominal Mach number 9 nozzle has been installed in the LDH tunnel. A small Mach number gradient, approximately 0.25 per inch, existed during the present tests. Free-stream conditions quoted are based on conditions at the model nose, and typical Mach number increases over the length of the test model amount to approximately 4 percent. The repeatability of the drag measurements was found to be about ± 5 percent, and the overall uncertainty is expected to be within ± 10 percent.

3.3 50-INCH MACH 10 TUNNEL (C) DATA

Uncertainties resulting from the gas properties and assumptions used in inferring flow conditions are, of course, markedly reduced in this essentially perfect gas facility as compared to the previously discussed hypervelocity facilities. The dominant uncertainties are the drag measurement, which had a repeatability of ± 5 percent, and the lack of accurate base pressure data. The Mach 10 drag data presented herein were corrected to an approximate zero-base drag condition by assuming that the base pressure was one-half of free-stream

static pressure. This correction ranged from -2 to -8 percent of the measured total drag.

4.0 THEORETICAL CONSIDERATIONS

4.1 SIMILAR SOLUTIONS

The similar solutions and integral method of Cohen and Reshotko (Refs. 12 and 13) were used to obtain a theoretical estimate of the Blasius-type shear stress distribution and hence total shear drag of the cones considered herein. The so-called "linear method" applicable when the surface temperature is constant, described in detail by Cohen and Reshotko in Ref. 13, was used with application of Mangler's transformation (Ref. 14) for the axisymmetric cones considered here. The starting point of the calculation was either (a) an axisymmetric stagnation point or (b) a sharp cone point. The initial starting point (a), referred to herein as the normal shock case, assumes that all of the fluid within and immediately adjacent to the boundary layer passed through the essentially normal portion of the bow shock wave. Starting point (b), referred to as the conical shock case, assumes conditions at the outer edge of the boundary layer equal to inviscid cone surface conditions. Certainly the normal shock approximation is expected to be valid for a sufficiently blunt body at a sufficiently high Reynolds number. For the blunt cones studied here, it is suggested and later supported by the experimental data that the cones with bluntness ratios $\psi \geq 0.3$ are sufficiently blunt. Application of the conical shock case to the present study is less clear. Shock wave curvature (hence vorticity in the cone flow field) occurs because of the "aerodynamic" bluntness induced by the boundary layer. The dominant influence of small degrees of nose bluntness at hypersonic speeds has been discussed and illustrated in the literature (e.g., Ref. 15, pp. 6-7). In general, the vorticity introduced into the flow field by the curved bow shock wave should be accounted for in the boundary-layer calculations; however, a detail analysis including vorticity is quite complex and is not considered here.

Although nitrogen is a nearly perfect gas within the range of temperature considered herein ($T_0 \leq 4000^\circ\text{K}$), small and possibly accumulative inconsistencies arise in the comparison of perfect gas theoretical results and experiments in real nitrogen. To avoid these inconsistencies, real nitrogen thermodynamic and transport properties, as described by Grabau, et. al. (Ref. 11), were used in the theoretical calculations for the hypervelocity test conditions of the hotshot tunnels. Perfect gas calculations are used for comparison with the lower temperature

($T_0 \sim 1900^\circ\text{R}$) air tests in the 50-Inch Mach 10 Tunnel (C). Both the real nitrogen and perfect gas boundary-layer calculations, using Cohen and Reshotko's integral method (Ref. 13), were performed on an IBM 7070 computer.

The calculation of skin-friction coefficients (based on free-stream properties) by the integral method requires knowledge of the free-stream conditions, model geometry, and pressure distribution (and hence pressure gradient distribution). The correlation of characteristics solutions and measured pressure distributions given by Lewis (Ref. 3), in terms of parameters proposed by Cheng (Ref. 16), was used to specify the pressure distributions for the blunter ($\psi \geq 0.3$) cones. Lewis' data were replotted in terms of pressure coefficient (Fig. 7) and then were assumed independent of Mach number for this application. For the sharper cones ($\psi \leq 0.03$) the normal shock case was treated by neglecting the small regime of adverse pressure gradient and using a smooth transition between a hemispherical nose pressure distribution and the inviscid, sharp cone, pressure level. Experimental cone pressure data from Whitfield and Norfleet (Ref. 4) were used to specify the inviscid cone pressure, and the resulting pressure distribution for the sharper cones ($\psi \leq 0.03$) is shown in Fig. 8. The conical shock case simply assumes that the cone surface pressure is constant at the inviscid value given in Ref. 4.

The average skin-friction coefficients calculated by the integral method for a given geometry, wall temperature, and test gas were found to correlate as a linear function of the viscous parameter.

$$\bar{v}_\infty = \frac{\sqrt{C_\infty} M_\infty}{\sqrt{Re_\infty L}} \quad (1)$$

thus

$$\bar{C}_{Df} = A \bar{v}_\infty \quad (2)$$

Values of A obtained by the integral method are listed in Table 2 for both the normal and conical shock cases considered.

4.2 VISCOUS INTERACTION EFFECTS

The previous results from the similar solutions are based on the thin boundary-layer concept, and thus no interaction between the viscous and inviscid flow fields is considered in these solutions. It will be seen that although the major portion of the experimentally observed viscous drag rise is accounted for by the similar solutions, viscous drag rises

consistently greater than predicted by the similar solutions are observed. Consideration of viscous interaction effects leads one to expect that such will occur.

It has been shown by Lees and Probstein (Ref. 17) that the two-dimensional flow over a wedge or flat-plate divides quite naturally into the so-called "strong" and "weak" interaction zones. The "strong" interaction regime is characterized by large induced pressure gradients which have an important effect on the boundary-layer growth and necessitate consideration of the mutual interaction between the boundary layer and the boundary-layer induced pressure gradients; in the "weak" interaction regime, the induced pressure gradient does not have an important influence on the boundary-layer growth, and the effects are essentially perturbations of the thin boundary-layer solution. Probstein's (Ref. 18) (see also Probstein and Elliott, Ref. 19) analysis for the analogous weak interaction field for the axially symmetric flow over a cone is used here to estimate the viscous interaction influence. The present consideration of only "weak" interactions is based on the fact that the displacement thickness in the axisymmetric case will be markedly reduced as compared to the flat-plate case, and it is implied that the weak interaction flow regime covers a larger range over the cone. Also, as concluded by Probstein (Ref. 18) and illustrated later by the estimates made herein, the dominant induced effect in the present continuum regime arises from transverse curvature considerations. Although a strong interaction regime must always exist near the nose, this regime has been neglected herein. It should be noted that the theoretical treatment of the flow regime in the immediate vicinity of the nose (or leading edge) is far from satisfactory, even in the two-dimensional flat-plate case. The fact that the strong interaction becomes invalid in the immediate vicinity of the leading edge has been recognized by several authors in the literature (e.g., Lees and Probstein, Ref. 17; Oguchi, Refs. 20 and 21).

Although experimental data are presented herein where strong interaction effects, vorticity effects, slip and wall temperature jump effects are likely present, the theoretical considerations are restricted to the continuum weak interaction regime.

The characteristic nature of the boundary layer on a body of revolution differs from that on a flat-plate shape in that the axisymmetric boundary layer must spread circumferentially as it grows in thickness with distance along the surface. The displacement thickness of the boundary layer gives rise, in the axisymmetric case, to induced effects in two planes, i.e., in the median plane associated with the longitudinal boundary-layer growth and in a plane perpendicular to the axis of symmetry. The longitudinal boundary-layer induced effects may be treated

by using Mangler's transformation (Ref. 14) to transform the equations of motion for the boundary layer on an axisymmetric body to those on a flat-plate, provided the thickness of the boundary layer is negligible compared with the body radius and then considering a "weak" interaction perturbation of this classical solution, as accomplished by Probstein (Ref. 17). A transverse-curvature-induced effect arises when the boundary-layer thickness is not negligible compared to the body radius. Probstein (Ref. 18), Probstein and Elliott (Ref. 19), and Yasuhara (Ref. 22) have considered this problem for slender axisymmetric bodies. The works of Probstein (Ref. 18) and Probstein and Elliott (Ref. 19) are followed here to make estimates of the longitudinal and transverse-induced effects. Yasuhara's work is not used here because of his requirement for locally hypersonic flow conditions, a condition not usually obtained on blunt cones even at hypersonic flight Mach numbers.

4.2.1 Displacement-Induced Pressure Drag

The induced local pressure rise caused by the boundary-layer displacement thickness is given by Probstein as (in terms of present nomenclature):

$$\frac{\Delta p}{p_e} = F_1(K) d_\infty \bar{X} + F_2(K) d_\infty^2 \bar{X}^2 \quad (3)$$

where for $P_r = 1$, $\gamma = 1.4$

$$d_\infty = 0.2 (T_w/T_o) + 0.066$$

and

$$K = M_\infty \theta_c$$

and the functions $F_1(K)$ and $F_2(K)$ have been computed and presented by Probstein (Ref. 18). The induced pressure drag may be obtained by integrating Eq. (3) over the cone surface, assuming constant surface flow properties (inviscid local properties at $x = L$ were used herein). In terms of an incremental drag coefficient the result is, to first order*

$$(\Delta C_D)_p = \frac{4}{3} \bar{C}_{p_e} F_1(K) d_\infty \bar{X}_1 \quad (4a)$$

For a given cone and a limited range of free-stream conditions (e. g., tests in one wind tunnel) the local viscous interaction parameter,

*For the slender cones considered here, it is assumed that $s = x$ or $\cos \theta_c \approx 1$.

$\bar{X}_L \equiv \sqrt{C_e} M_e^3 / \sqrt{(\rho_e u_e L) / \mu_e}$, can be shown to be proportional to the free-stream viscous parameter,

$$\bar{v}_\infty \equiv \frac{\sqrt{C_\infty} M_\infty}{\sqrt{Re_{\infty, L}}}$$

or,

$$\bar{X}_L = \frac{M_e}{\sqrt{\frac{\gamma_\infty / p_e}{p_o}}} \left(\frac{u_e}{u_\infty} \right)^{3/2} \frac{\sqrt{C_\infty} M_\infty}{\sqrt{Re_{\infty, L}}} = B \bar{v}_\infty \quad (5)$$

Therefore, Eq. (4a) may be written as

$$(\Delta C_D)_p \approx \frac{4}{3} \bar{C}_{p_e} F_1(K) d_\infty B \bar{v}_\infty \quad (4b)$$

Values of the proportionality constant B are given in Table 2 for the cases considered herein.

4.2.2 Displacement-Induced Friction Drag

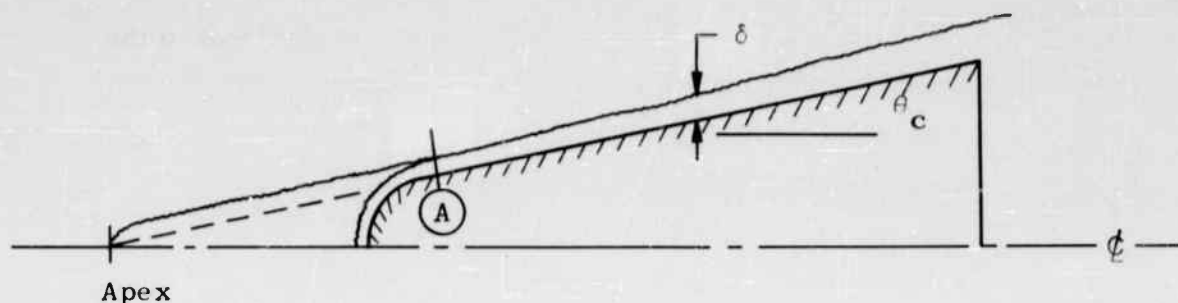
The pressure gradient induced by the boundary-layer displacement thickness gives rise to an induced friction drag, referred to herein as the "displacement-induced friction". The displacement-induced friction is given by Probstein as (in present nomenclature):

$$\frac{(\Delta C_{Df})_p}{\bar{C}_{Df}} = \left[\frac{-0.823}{M_e^2} + \frac{0.524}{M_e^2} \left(\frac{T_w}{T_o} \right) + 0.761 \right] d_\infty F_1(K) \bar{X} \quad (6)$$

Therefore, the total induced friction will be for constant surface flow properties,

$$\frac{(\Delta C_{Df})_p}{\bar{C}_{Df}} = \frac{3}{2} \left[\frac{-0.823}{M_e^2} + \frac{0.524}{M_e^2} \left(\frac{T_w}{T_o} \right) + 0.761 \right] d_\infty F_1(K) B \bar{v}_\infty \quad (7)$$

This analysis applies only to the sharp cone case and is expected to overestimate the increase in skin friction for the blunt cone case if applied directly as written in Eq. (7). A crude but simple correction for small degrees of nose bluntness can be made by assuming that the local induced friction at the beginning of the truncated conical section is the same as would exist at this point for the sharp case. Consider the sketch shown on the following page:



Integrating from point (A) to the cone base, again assuming constant local properties and neglecting higher order terms of the bluntness ratio, ψ , the following simple correction is obtained:

$$\frac{(\Delta C_{Df})_p}{\bar{C}_{Df}} = (1 - \psi) \frac{3}{2} \left[\frac{-0.823}{M_e^2} + \frac{0.524}{M_e^2} \left(\frac{T_w}{T_o} \right) + 0.761 \right] d_\infty F_1(K) B \bar{v}_\infty \quad (8)$$

This correction for nose bluntness was applied herein to all nose bluntnesses considered, conditions under which the approximation is admittedly quite poor. The justification here lies in the fact that the induced terms are in themselves not large, and an approximate correction, argued to be in the correct direction, is applied to these second-order effects.

4.2.3 Transverse-Curvature-Induced Friction Drag

The local induced friction caused by transverse curvature is given by Probstein as (in present nomenclature):

$$\frac{(\Delta c_f)_{tc}}{\bar{c}_f} = \left[\frac{0.517}{M_e^2} + \frac{0.913}{M_e^2} \left(\frac{T_w}{T_o} \right) + 0.183 \left(\frac{T_w}{T_o} \right) + 0.048 \right] \frac{\bar{X}}{\sqrt{3} M_e \theta_c} \quad (9)$$

Integrating over the cone surface and again following the bluntness effect correction applied above, the total induced friction caused by transverse curvature is obtained as,

$$\frac{(\Delta C_{Df})_{tc}}{\bar{C}_{Df}} = (1 - \psi) \frac{3}{2} \left[\frac{0.517}{M_e^2} + \frac{0.913}{M_e^2} \left(\frac{T_w}{T_o} \right) + 0.183 \left(\frac{T_w}{T_o} \right) + 0.048 \right] \frac{B \bar{v}_\infty}{\sqrt{3} M_e \theta_c} \quad (10)$$

4.3 TOTAL ZERO-LIFT DRAG ESTIMATE

The total zero-lift drag estimate consists of the following terms:

1. inviscid pressure drag, C_{D_o}
2. similar friction drag, \bar{C}_{D_f}
3. displacement-induced pressure drag, $(\Delta C_D)_p$
4. displacement-induced friction drag, $(\Delta C_{D_f})_p$
5. transverse-curvature-induced friction drag, $(\Delta C_{D_f})_{tc}$

Thus, the total zero-lift drag becomes, with zero base drag:

$$C_D = C_{D_o} + (\Delta C_D)_p + \bar{C}_{D_f} \left[1 + \frac{(\Delta C_{D_f})_p}{\bar{C}_{D_f}} + \frac{(\Delta C_{D_f})_{tc}}{\bar{C}_{D_f}} \right] \quad (11)$$

Examination of the various equations for each of the above terms reveals that it is necessary to specify for each perfect gas case to be considered; γ , $C_p(x)$, (T_w/T_o) , ψ , θ_c , and the condition of conical or normal shock wave. These specifications will permit the calculation of each drag term in the perfect gas case. Of course, when departures from a perfect gas are to be considered, the specific flow condition must be completely defined. As noted before, the perturbation terms were computed assuming constant local flow properties. Inviscid flow conditions at $x = L$ were used for these estimates.

It should be noted again here that the above estimate assumes a weak interaction model and thus ignores the strong interaction regime near the nose. Effects associated with flow field vorticity or with conditions where the molecular mean free path is comparable to body dimensions are not considered; thus, large values of the viscous parameter, \bar{v}_∞ , cannot be considered. This limitation will be illustrated later by comparison with experimental data.

The primary cone model used in the experimental study is considered here in detail to illustrate the relative magnitudes of the various terms of Eq. (11). This model is a blunt ($\psi = 0.3$), slender ($\theta_c = 9$ deg) cone considered under hypersonic ($M_\infty = 19$) cold-wall ($T_w/T_o = 0.1$) conditions with nitrogen as a test gas. The resulting breakdown of Eq. (11) becomes

under these conditions:

$$\begin{aligned}
 C_D = & 0.130 \text{ (inviscid pressure drag)} \\
 & + 1.09 \bar{v}_\infty \text{ (similar friction drag)} \\
 & + 0.03 \bar{v}_\infty \text{ (displacement-induced pressure drag)} \\
 & + 0.47 \bar{v}_\infty^2 \text{ (displacement-induced friction drag)} \\
 & + 2.34 \bar{v}_\infty^2 \text{ (transverse-curvature-induced friction drag)}
 \end{aligned}$$

This drag estimate is illustrated in Fig. 9. For this case it is noted that the similar or Blasius-type friction drag quickly comes to dominate the zero-lift drag with decreasing Reynolds number (i. e., increasing \bar{v}_∞). In general, it is found for the cold-wall case that the displacement-induced pressure drag and the displacement-induced friction drag terms are small compared to the other terms. For the hot-wall case, the displacement-induced friction drag and the transverse-curvature-induced friction drag terms become comparable. Drag estimates based on the above, outlined procedures are compared to the experimental data in the following section.

5.0 EXPERIMENTAL RESULTS

Preliminary drag data from the present research were previously published by Lukasiewicz, Whitfield, and Jackson (Ref. 2). The present data should be taken to supersede these earlier data because of better definition of test conditions. For example, the sharp cone pressure distributions published by Lewis (Ref. 3) were found to be affected by source flow effects caused by the use of conical nozzles (see Ref. 4), and the definition of total enthalpy level has been improved (see section 3.1).

The experimental forebody drag data used herein are presented in tabular form as Appendix I and are compared with the theoretical estimates in graphical form. The presentation of tabular drag data is made to facilitate future comparisons between theory and experiment. The theoretical models used herein are considered far from adequate, as noted below, to explain all the available data. Future comparisons with more exact theoretical estimates are encouraged.

Experimental total drag data are used herein for Mach numbers greater than 10 since the base drag is negligible for these test conditions.

The experimental drag data for Mach number 10 and less (i. e., the 50-Inch Mach 10 Tunnel (C) and Hypervelocity Low-Density Tunnel data) were corrected to an approximate zero base drag condition by assuming that the base pressure was one-half free-stream static pressure. Attempts to measure these base pressures were unsuccessful; however, it is expected that the model base pressures are at least one-half free-stream pressure.

The theoretical drag estimates considered previously indicate that the total drag of a slender cone should correlate with the viscous parameter, $\bar{v}_\infty = (\sqrt{C_\infty} M_\infty) / \sqrt{Re_\infty L}$. The experimental forebody drag data from 6.34-, 9-, 13.5-deg cones obtained within the continuum flow regime are presented as a function of the viscous parameter \bar{v}_∞ in Figs. 10, 11, and 12, respectively. Theoretical estimates based on the normal shock wave theoretical model are presented in all cases, and in addition, a conical shock estimate is presented for the hot-wall, sharper 9-deg cone case (Fig. 11a). Experimental data from the Cornell Aeronautical Laboratory's 48-Inch Contoured Nozzle Shock Tunnel (Ref. 23) obtained with air as a test gas and under cold-wall, hypersonic flow conditions are also included in Figs. 10a and 11. These data are in good agreement with the hotshot data and with the theoretical estimates. Also included in Fig. 11 are hot-wall drag data obtained in the Jet Propulsion Laboratory's 21-inch hypersonic wind tunnel by Aerodynamic (Ref. 24). Reference 24 does not mention the model base pressure; however, it was assumed that the data represented total drag measurements. A base pressure of one-half free-stream static pressure was assumed, and the drag data were corrected accordingly. The specific wall to stagnation temperature ratios for the data of Ref. 24 are unknown; however, it is reasonable to assume that the ratios for steady-state conditions are comparable to the present Mach 10, hot-wall ($T_w/T_0 \sim 0.75$) data.

The good agreement between the normal shock drag estimates and experiment for all of the cold-wall data in Figs. 10, 11, and 12 must be considered, at present, fortuitous for the sharper 6.34- and 9-deg cones. Certainly, the normal shock theoretical model is violated for these sharper cone cases. An experimental check was made on the drag of a quite sharp 9-deg cone, and these data are included in Fig. 11a as solid symbols. Experimentally, the difference in the drag of a "sharp" ($\psi \sim 0$) cone and one with a small bluntness ($\psi = 0.03$) could not be detected. Although arguments on the influence of "aerodynamic" bluntness can be advanced, further theoretical work is required to sort out the influence of vorticity in these cases. It is interesting to note that in spite of the mismatch between the theoretical and experimental sharper ($\psi \leq 0.03$)

cone models, a good engineering approximation of the total drag within the continuum flow regime can be made by the methods presented herein. Certainly the agreement between the theoretical and experimental models is much better for the blunter ($\psi \geq 0.3$) cones, and again the theoretical model offers a good estimate of the total drags (see Figs. 10b, 11b, and 12).

The hot-wall, sharp and blunt cone drag data are also presented in Figs. 11 and 12. The experimental data are observed to be consistently above the theoretical estimates for all models. It should be noted that the low absolute drag level required special techniques of measurement (see section 2.2). Although the repeatability of these measurements was less than the differences between theory and experiment observed, the absolute or fixed errors in the experiment cannot be assumed small enough to permit an assessment of the lack of validity of the hot-wall theory.

Experimental drag data obtained under cold-wall, low-density hypersonic conditions in the LDH tunnel are compared to the higher Reynolds number data and continuum theory in Fig. 13. Continuum theoretical estimates based on the present theoretical model and corresponding to the low-density test conditions were not made because of the obviously poor match between theoretical and experimental models. It is certainly to be expected that vorticity, slip, and temperature jump effects are present in these data in varying degrees. It is interesting to note from these drag data that the low-density ($\bar{v}_\infty > 0.3$) drag coefficients are essentially independent of the specific body shape. These data indicate that even very slender bodies will experience a drag level comparable to that of a sphere for $\bar{v}_\infty > 0.4$. Proper theoretical treatment of this important transition regime from continuum to free-molecular flow remains to be shown and is, of course, urgently needed to better understand the flow phenomena.

6.0 CONCLUDING REMARKS

Comparison of viscous-dominated drag data from blunt slender cones with estimates based on the theoretical work of Cohen and Reshotko and Probstein indicates good agreement for moderate values of the viscous parameter \bar{v}_∞ (≥ 0.15). Agreement between theoretical estimates based on the blunt model (normal shock theory) and the experimental cold-wall data from sharp cones must be considered, at present, fortuitous. Similar agreement was not found for the hot-wall, sharper cone data.

The theoretical estimates for the blunt slender cones under cold-wall, hypersonic, continuum flow conditions indicate that the dominant viscous contribution is simply the "Blasius" or similar friction drag. The primary perturbation of this similar friction drag, for this cold-wall situation, arises from transverse curvature effects with a relatively small influence introduced by the displacement-induced longitudinal pressure gradient. It is interesting that time-honored methods of compressible boundary-layer analysis serve to offer a reasonable engineering approximation to these quite large viscous drag rises.

Within the range of blunt cone geometries studied experimentally under low-density hypersonic conditions, a significant influence of geometry was not noted. Experimental drag levels near the inviscid drag of a sphere were observed for all of the cones under these low Reynolds number, cold-wall conditions.

REFERENCES

1. Lukasiewicz, J., Whitfield, Jack D. and Jackson, R. "Aerodynamic Testing at Mach Numbers 15 to 20." Hypersonic Flow Research, Vol. 7, Progress in Astronautics and Rocketry. pp. 473-512, Academic Press, 1962.
2. Lukasiewicz, J., Jackson, R. and Whitfield, Jack D. "Status of Development of Hotshot Tunnels at the AEDC." Paper presented at the AGARD Meeting on "High Temperature Aspects of Hypersonic Flow", Training Center for Experimental Aerodynamics, Rhode-Saint-Genese, Belgium, April 3-6, 1962.
3. Lewis, C. H. "Pressure Distribution and Shock Shape over Blunted Slender Cones at Mach Numbers 16 to 19." AEDC-TN-61-81, August 1961.
4. Whitfield, Jack D. and Norfleet, Glenn D. "Source Flow Effects in Conical Hypervelocity Nozzles." AEDC-TDR-62-116, June 1962.
5. Whitfield, Jack D. and Wolny, W. "Hypersonic Static Stability of Blunt Slender Cones." AEDC-TDR-62-166, August 1962.
6. Potter, J. Leith, Kinslow, Max, Arney, George D., Jr., and Bailey, Allan B. "Description and Preliminary Calibration of a Low-Density, Hypervelocity Wind Tunnel." AEDC-TN-61-83, August 1961.

7. Test Facilities Handbook, (4th Edition). "von Kármán Gas Dynamics Facility, Vol. 4." Arnold Engineering Development Center, July 1962.
8. Arney, George D. and Boylan, David E. "A Calorimetric Investigation of Some Problems Associated with a Low-Density Hypervelocity Tunnel." AEDC-TDR-63-19, February 1963.
9. Earheart, W. T., Jr. and Bynum, D. S. "Hypervelocity Arc-Tunnel Instrumentation." AEDC-TN-60-227, December 1960.
10. Fay, J. A. and Riddell, F. R., "Theory of Stagnation Point Heat Transfer in Dissociated Air." Journal of the Aeronautical Sciences, Vol. 25, No. 2, February 1958. pp. 73-85.
11. Grabau, Martin, Humphrey, Richard L., and Little, Wanda J. "Determination of Test-Section, After-Shock, and Stagnation Conditions in Hotshot Tunnels Using Real Nitrogen at Temperatures from 3000 to 4000°K." AEDC-TN-61-82, July 1961.
12. Cohen, Clarence B. and Reshotko, Eli. "Similar Solutions for the Compressible Laminar Boundary Layers with Heat Transfer and Pressure Gradient." NACA Report 1293, 1956.
13. Cohen, Clarence B. and Reshotko, Eli. "The Compressible Laminar Boundary Layer with Heat Transfer and Arbitrary Pressure Gradient." NACA Report 1294, 1956.
14. Mangler, W. "Compressible Boundary Layers on Bodies of Revolution." Interrogation Report, ATI No. 28063, MAP-VG 83-4.7. T, Translation, June 1946.
15. Hayes, Wallace D. and Probstein, Ronald F. Hypersonic Flow Theory. Academic Press, New York, 1959.
16. Cheng, H. K. "Hypersonic Flow with Combined Leading-Edge Bluntness and Boundary-Layer Displacement Effect." Cornell Aeronautical Laboratory Report No. AF-1285-A-4, AD 243140, August 1960.
17. Lees, Lester and Probstein, Ronald F. "Hypersonic Viscous Flow over a Flat Plate". Report No. 195, Aero Engineering Lab, Princeton University, April 20, 1952.
18. Probstein, Ronald F. "Interacting Hypersonic Laminar Boundary Layer Flow Over a Cone." Tech. Report AF 279811, Division of Engineering, Brown University, AD 66 227, March 1955.

19. Probst, Ronald F. and Elliott, David. "Transverse Curvature Effect in Compressible Axially Symmetric Laminar Boundary-Layer Flow." Journal of Aeronautical Sciences, Vol. 23, No. 3, March 1956.
20. Oguchi, H. "First-Order Approach to a Strong Interaction Problem in Hypersonic Flow over an Insulated Flat Plate." University of Tokyo Aero. Research Institute Report No. 330, Vol. 24, No. 1, June 1958.
21. Oguchi, H. "The Sharp Leading Edge Problem in Hypersonic Flow." Brown University, Division of Engineering, Report ARL TN 60-133, 1960.
22. Yasuhara, M. "Axisymmetric Viscous Flow Past Very Slender Bodies of Revolution." Journal of Aerospace Sciences, Vol. 29, No. 6, June 1962. p. 667-679.
23. Wilkison, D. B. and Harrington, S. A. "Hypersonic Force, Pressure and Heat Transfer Investigations of Sharp and Blunt Slender Cones." Cornell Aeronautical Laboratory. Report No. AF-1560-A-5, December 1962.
24. Aeronutronic, A Division of Ford Motor Company. "Experimental Investigation of the Aerodynamic Characteristics of 9° Half-Angle Cones with Varying Degrees of Nose Bluntness at Mach Number 9." Pub. No. U-1638, April 1962.

APPENDIX I
TABULATED ZERO-LIFT DRAG DATA

Model	θ_c	ψ	T_w/T_o	M_∞	$Re_{\infty,L}$	\bar{v}_∞	C_D
1	6.34°	0.03	0.1	14.7	150,500	.0353	.099
1	6.34°	0.03	0.1	16.2	572,000	.0200	.072
1	6.34°	0.03	0.1	17.2	161,000	.0399	.109
1	6.34°	0.03	0.1	17.4	338,000	.0278	.084
1	6.34°	0.03	0.1	17.5	258,000	.0321	.101
2	6.34°	0.30	0.1	15.9	412,000	.0231	.136
2	6.34°	0.30	0.1	16.9	172,000	.0379	.185
2	6.34°	0.30	0.1	17.5	109,000	.0494	.179
2	6.34°	0.30	0.1	18.0	224,400	.0354	.164
3	9°	~ 0	0.1	17.0	63,000	.0631	.167
3	9°	~ 0	0.1	18.0	47,800	.0765	.181
3	9°	~ 0	0.1	17.0	60,300	.0646	.181
3	9°	~ 0	0.1	17.0	42,200	.0771	.180
4	9°	0.03	0.1	22.4	257,000	.0414	.129
4	9°	0.03	0.1	21.0	99,200	.0621	.162
4	9°	0.03	0.1	21.6	507,000	.0283	.116
4	9°	0.03	0.1	22.0	245,000	.0414	.130
5	9°	0.03	0.1	17.4	247,000	.0326	.112
5	9°	0.03	0.1	16.1	395,400	.0238	.110
5	9°	0.03	0.1	17.4	122,400	.0463	.143
5	9°	0.03	0.1	17.2	143,800	.0423	.134
6	9°	0.03	0.1	22.4	84,600	.0717	.192
6	9°	0.03	0.1	21.0	32,700	.1081	.246
6	9°	0.03	0.1	21.6	167,000	.0493	.154
6	9°	0.03	0.1	22.0	80,700	.0721	.185
6	9°	0.03	0.1	21.8	44,000	.0967	.235
6	9°	0.03	0.1	21.4	26,300	.1230	.318
6	9°	0.03	0.1	21.0	18,300	.1445	.336

APPENDIX I (Continued)

Model	θ_c	ψ	T_w/T_o	M_∞	$Re_{\infty, L}$	\bar{v}_∞	C_D
7a	9°	0.03	0.75	19.18	240,900	.0169	.121
7a	9°	0.03	0.75	10.15	169,000	.0202	.120
7a	9°	0.03	0.75	10.19	318,730	.0148	.109
7a	9°	0.03	0.75	10.19	321,400	.0147	.101
7a	9°	0.03	0.75	10.19	165,200	.0204	.111
7a	9°	0.03	0.75	10.15	166,600	.0204	.120
7a	9°	0.03	0.75	10.07	67,400	.0318	.148
7a	9°	0.03	0.75	10.04	39,400	.0414	.167
7a	9°	0.03	0.75	10.07	66,809	.0346	.148
7a	9°	0.03	0.75	10.04	39,100	.0416	.181
7a	9°	0.03	0.75	10.02	29,800	.0474	.208
7b	9°	0.03	0.20	9.23	818	.2728	.704
7b	9°	0.03	0.20	9.23	818	.2728	.712
7b	9°	0.03	0.20	9.00	883	.2570	.663
7b	9°	0.03	0.20	8.77	959	.2413	.637
7b	9°	0.03	0.20	8.77	959	.2413	.625
7b	9°	0.03	0.25	9.66	1529	.2120	.567
7b	9°	0.03	0.25	9.66	1529	.2120	.572
7b	9°	0.03	0.25	9.40	1657	.1983	.556
7b	9°	0.03	0.25	9.40	1657	.1983	.551
7b	9°	0.03	0.25	9.13	1807	.1845	.526
7b	9°	0.03	0.25	9.13	1807	.1845	.515
8	9°	0.30	0.1	19.8	245,000	.0372	.175
8	9°	0.30	0.1	21.2	176,000	.0471	.190
8	9°	0.30	0.1	20.2	232,000	.0390	.185
8	9°	0.30	0.1	18.6	94,100	.0652	.214
9	9°	0.30	0.1	16.3	253,000	.0302	.173
9	9°	0.30	0.1	17.0	81,200	.0557	.199
9	9°	0.30	0.1	17.1	82,300	.0556	.200
9	9°	0.30	0.1	18.0	126,000	.0472	.189
10a	9°	0.30	0.1	17.7	67,000	.0635	.200
10a	9°	0.30	0.1	17.9	73,500	.0616	.208
10a	9°	0.30	0.1	17.8	71,300	.0598	.206
10a	9°	0.30	0.1	15.8	90,000	.0491	.186
10a	9°	0.30	0.1	16.8	30,300	.0896	.260
10a	9°	0.30	0.1	17.0	29,200	.0924	.250
10a	9°	0.30	0.1	17.0	27,900	.0939	.245
10a	9°	0.30	0.1	15.3	102,300	.0463	.182

APPENDIX 1 (Continued)

Model	θ_c	ψ	T_w/T_o	M_∞	$Re_{\infty, L}$	\bar{v}_∞	C_D
10b	9°	0.30	0.1	19.8	81,000	.0646	.230
10b	9°	0.30	0.1	21.5	57,100	.0838	.250
10b	9°	0.30	0.1	20.2	76,600	.0680	.228
11a	9°	0.30	0.75	10.15	126,000	.0235	.189
11a	9°	0.30	0.75	10.19	240,000	.0171	.169
11a	9°	0.30	0.75	10.18	179,900	.0198	.182
11a	9°	0.30	0.75	10.18	210,800	.0182	.165
11a	9°	0.30	0.75	10.10	64,000	.0327	.192
11a	9°	0.30	0.75	10.07	58,000	.0335	.200
11a	9°	0.30	0.75	10.07	49,200	.0372	.207
11a	9°	0.30	0.75	10.03	29,280	.0482	.235
11a	9°	0.30	0.75	10.00	15,140	.0665	.286
11a	9°	0.30	0.75	10.02	22,300	.0552	.259
11b	9°	0.30	0.20	9.23	610	.3161	.760
11b	9°	0.30	0.20	9.23	610	.3161	.758
11b	9°	0.30	0.20	9.23	610	.3161	.772
11b	9°	0.30	0.20	9.00	658	.2978	.724
11b	9°	0.30	0.20	9.00	658	.2978	.731
11b	9°	0.30	0.20	8.77	714	.2796	.699
11b	9°	0.30	0.20	8.77	714	.2796	.684
11b	9°	0.30	0.20	8.77	714	.2796	.696
11b	9°	0.30	0.25	9.66	1139	.2456	.642
11b	9°	0.30	0.25	9.66	1139	.2456	.648
11b	9°	0.30	0.25	9.40	1235	.2297	.590
11b	9°	0.30	0.25	9.40	1235	.2297	.608
11b	9°	0.30	0.25	9.13	1346	.2138	.577
11b	9°	0.30	0.25	9.13	1346	.2138	.585
11b	9°	0.30	0.25	9.13	1346	.2138	.565
12	13.5°	0.38	0.1	17.9	202,000	.0371	.247
12	13.5°	0.38	0.1	17.5	205,000	.0360	.255
12	13.5°	0.38	0.1	17.8	184,000	.0386	.265
13	13.5°	0.38	0.1	17.6	51,800	.0722	.273
13	13.5°	0.38	0.1	18.1	61,000	.0685	.275
13	13.5°	0.38	0.1	17.3	15,100	.1310	.340
13	13.5°	0.38	0.1	17.2	21,500	.1100	.322
13	13.5°	0.38	0.1	17.4	28,500	.0960	.305

APPENDIX I (Concluded)

Model	θ_c	ψ	T_w/T_o	M_∞	$Re_{\infty, L}$	\bar{v}_∞	C_D
14a	13.5°	0.30	0.75	10.15	78,960	.0296	.291
14a	13.5°	0.30	0.75	10.19	151,400	.0214	.266
14a	13.5°	0.30	0.75	10.18	113,800	.0248	.263
14a	13.5°	0.30	0.75	10.10	40,980	.0406	.278
14a	13.5°	0.30	0.75	10.04	18,400	.0606	.315
14a	13.5°	0.30	0.75	10.04	18,400	.0606	.336
14a	13.5°	0.30	0.75	10.07	30,600	.0472	.299
14a	13.5°	0.30	0.75	10.02	14,290	.0685	.339
14b	13.5°	0.38	0.20	9.23	381	.4000	.836
14b	13.5°	0.38	0.20	9.23	381	.4000	.837
14b	13.5°	0.38	0.20	9.00	411	.3768	.789
14b	13.5°	0.38	0.20	9.00	411	.3768	.794
14b	13.5°	0.38	0.20	8.77	446	.3538	.725
14b	13.5°	0.38	0.20	8.77	446	.3538	.756
14b	13.5°	0.38	0.25	9.66	712	.3108	.702
14b	13.5°	0.38	0.25	9.66	712	.3108	.664
14b	13.5°	0.38	0.25	9.66	712	.3108	.715
14b	13.5°	0.38	0.25	9.40	771	.2907	.678
14b	13.5°	0.38	0.25	9.40	771	.2907	.672
14b	13.5°	0.38	0.25	9.13	841	.2706	.642
14b	13.5°	0.38	0.25	9.13	841	.2706	.650

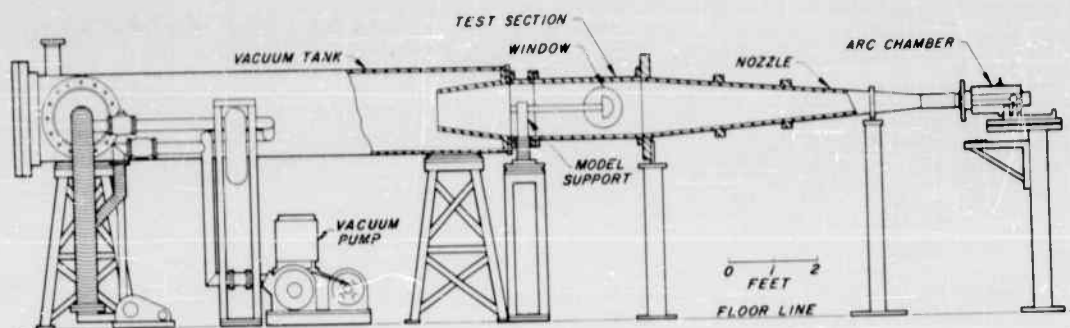
TABLE 1
VKF CONE DRAG MODELS

Model	θ_c	ψ	d_B , in.	VKF Tunnel	Test Gas	T_w/T_o	C_{D_o}
1	6.34	0.03	2.50	16-in. hotshot	N ₂	.1	.030
2	6.34	0.30	2.50	16-in. hotshot	N ₂	.1	.104
3	9	~0	0.985	16-in. hotshot	N ₂	.1	.060
4	9	0.03	3.00	50-in. hotshot	N ₂	.1	.063
5	9	0.03	2.50	16-in. hotshot	N ₂	.1	.063
6	9	0.03	0.985	50-in. hotshot	N ₂	.1	.063
7a	9	0.03	0.50	50-in. Mach 10	Air	~.75	.063
7b	9	0.03	0.50	LDH*	N ₂	.2-.25	.063
8	9	0.30	3.00	50-in. hotshot	N ₂	.1	.130
9	9	0.30	2.50	16-in. hotshot	N ₂	.1	.130
10a	9	0.30	0.97	16-in. hotshot	N ₂	.1	.130
10b	9	0.30	0.97	50-in. hotshot	N ₂	.1	.130
11a	9	0.30	0.50	50-in. Mach 10	Air	~.75	.130
11b	9	0.30	0.50	LDH*	N ₂	.2-.25	.130
12	13.5	0.38	4.00	16-in. hotshot	N ₂	.1	.220
13	13.5	0.38	1.10	16-in. hotshot	N ₂	.1	.220
14a	13.5	0.38	0.50	50-in. Mach 10	Air	~.75	.220
14b	13.5	0.38	0.50	LDH*	N ₂	.2-.25	.220

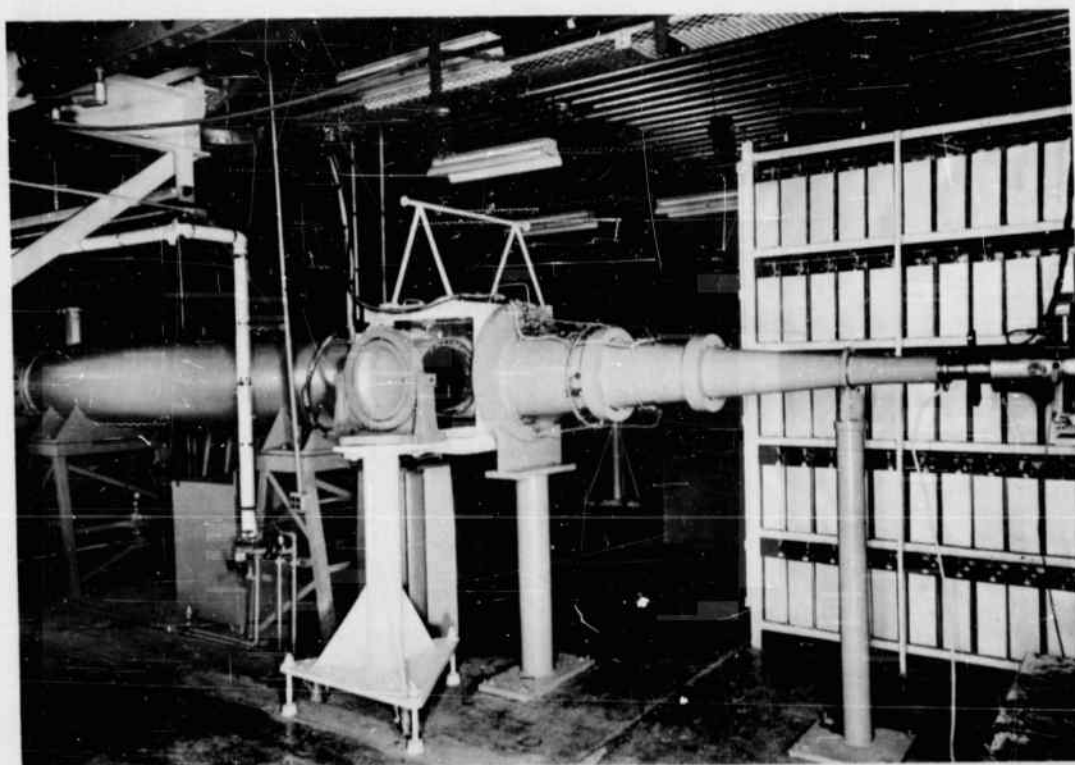
* Low-Density Hypervelocity Tunnel

TABLE 2
RESULTS FROM SIMILAR SOLUTIONS

θ_c , deg	ψ	Fluid	T_w/T_o	A	M_∞	B	$(M_e)_L$
(a) Normal Shock Case							
6.3	0.03	N ₂	0.10	1.55	19	13.9	3.01
	0.30	N ₂	0.10	1.18	19	17.9	3.24
9	0.03	N ₂	0.10	1.45	19	8.1	2.64
	0.03	Air	0.75	1.58	10	8.5	2.71
9	0.30	N ₂	0.10	1.09	19	11.2	2.85
	0.30	Air	0.75	1.45	10	11.1	2.92
13.5	0.38	N ₂	0.10	.71	19	5.9	2.44
	0.38	Air	0.75	.94	10	6.5	2.50
(b) Conical Shock Case ($\psi = 0$)							
$\gamma_e = \gamma_\infty = 1.4$; $M_\infty = 10$; $\theta_c = 9^\circ$; $u_e = u_\infty$; $\bar{C}_{Df} = 2 \bar{v}_\infty$;							
$\bar{x}_L = 33 \bar{v}_\infty$; $M_e = 7$							

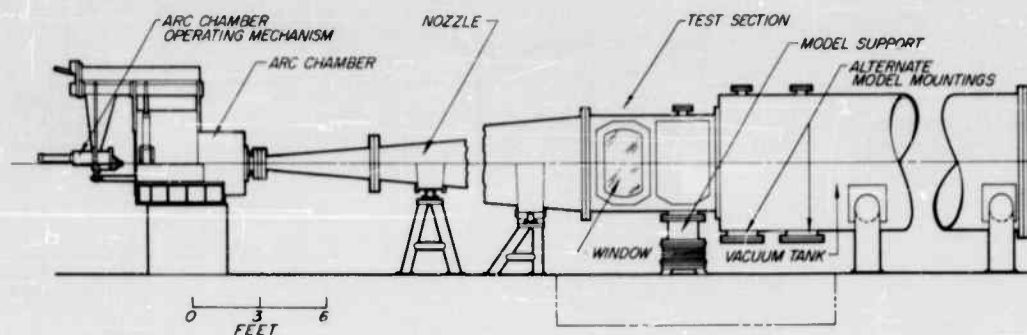


Assembly

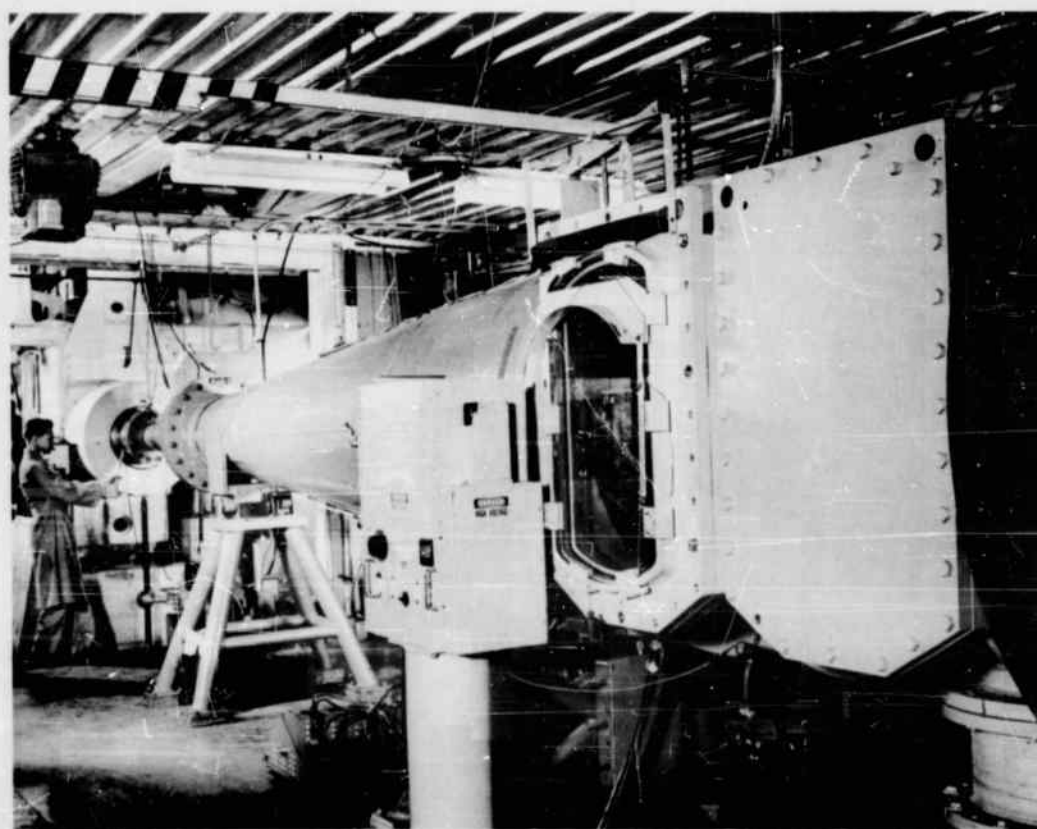


Arc Chamber, Nozzle, and Test Section

Fig. 1 The 16-Inch Hypervelocity Tunnel (Hotshot 1)

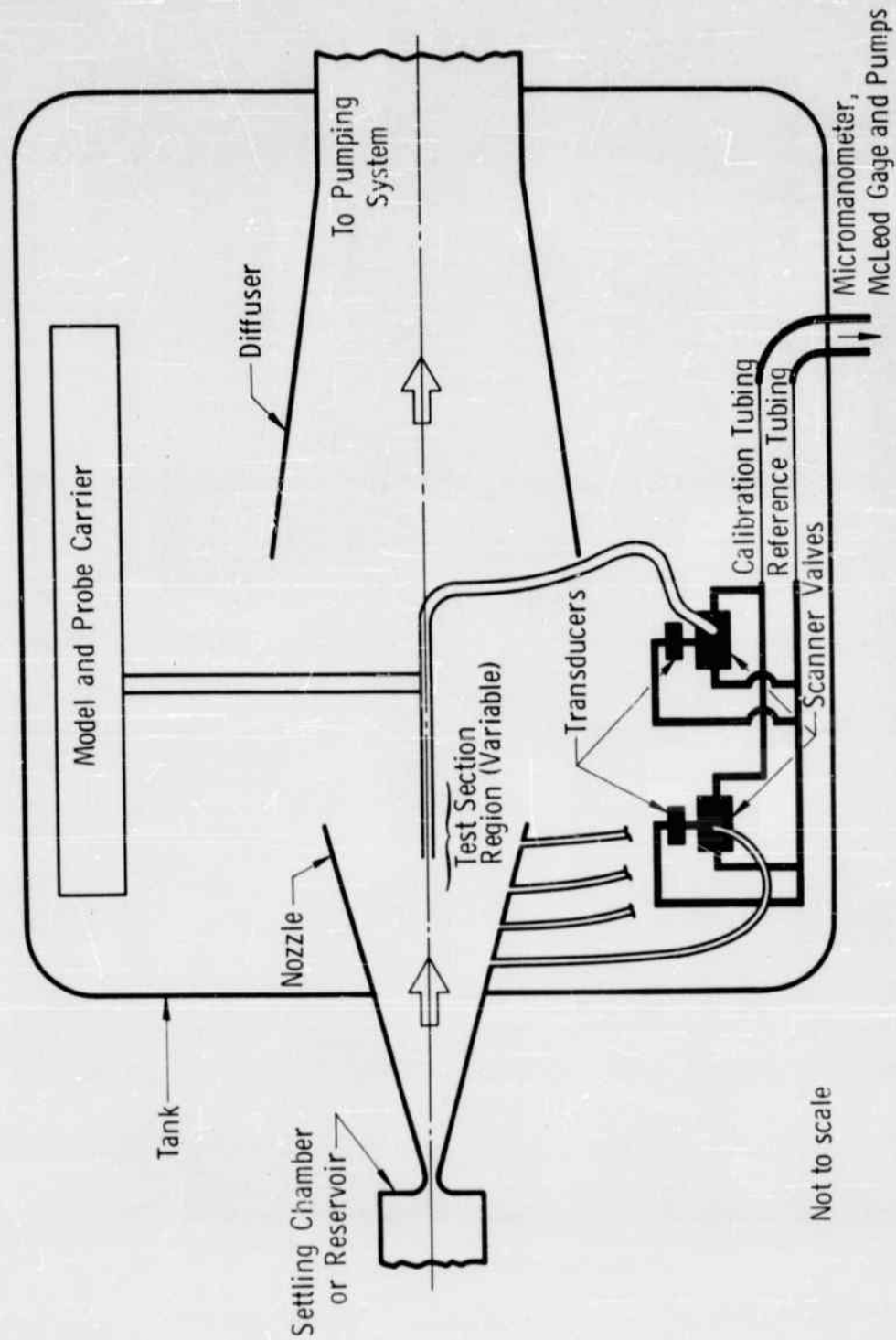


Assembly



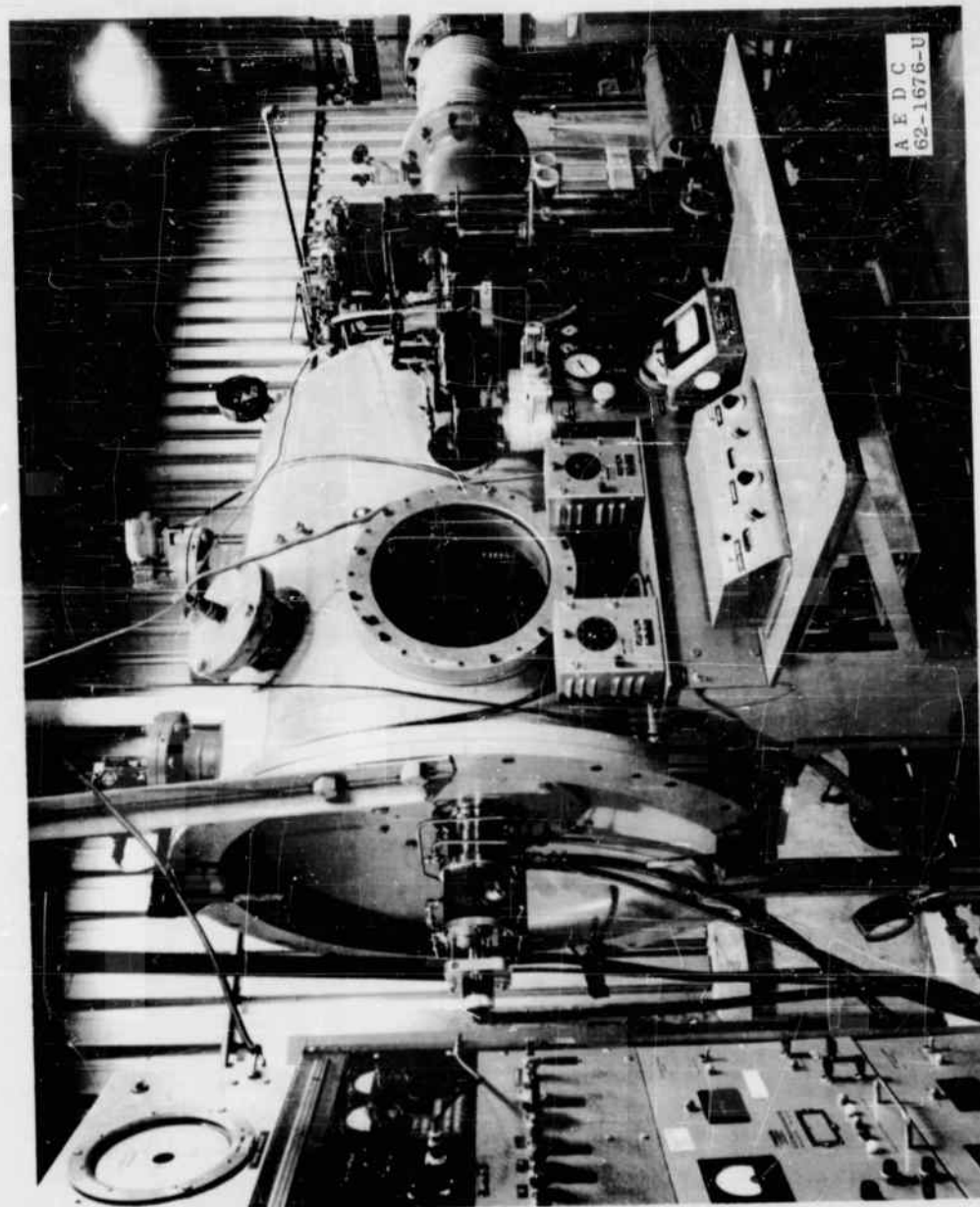
Arc Chamber, Nozzle, and Test Section

Fig. 2 The 50-Inch Hypervelocity Tunnel (Hotshot 2)

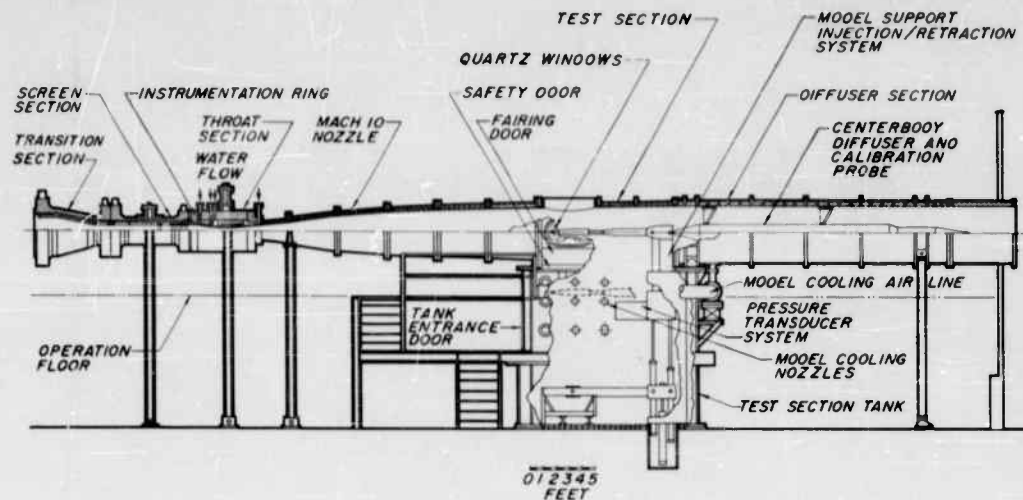


a. Schematic

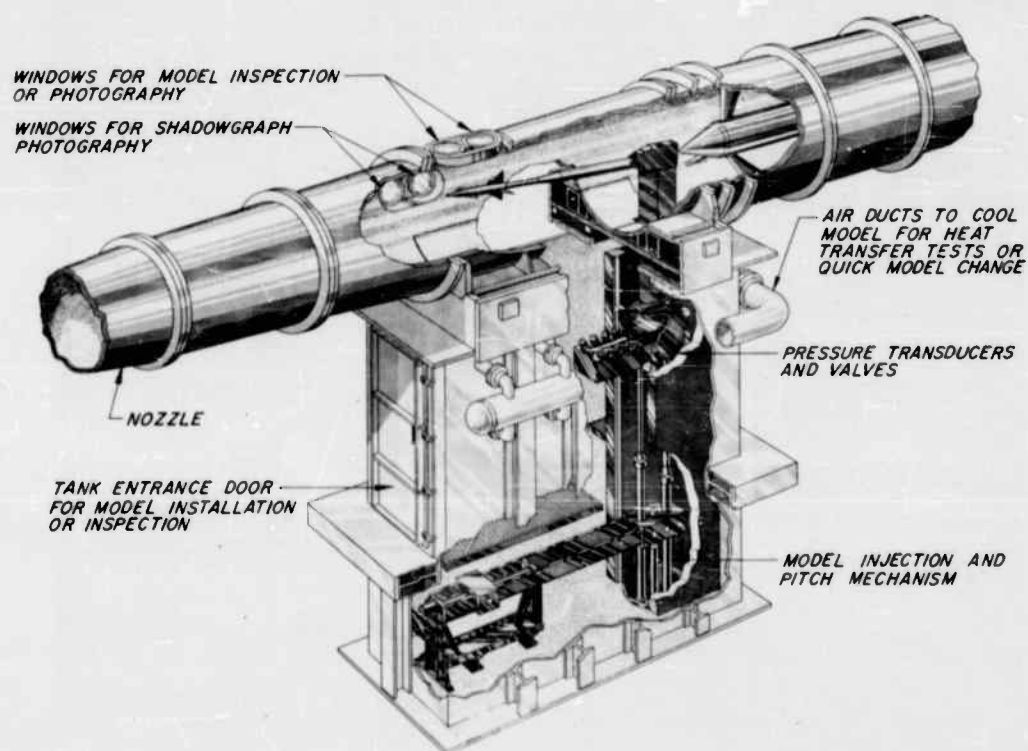
Fig. 3 Low-Density Hypervelocity Wind Tunnel



b. Photograph
Fig. 3 Concluded

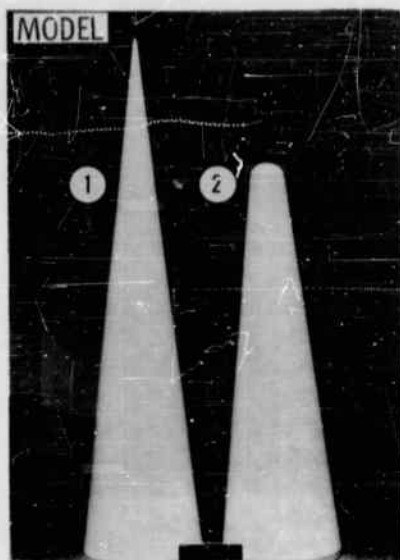


a. Tunnel Assembly

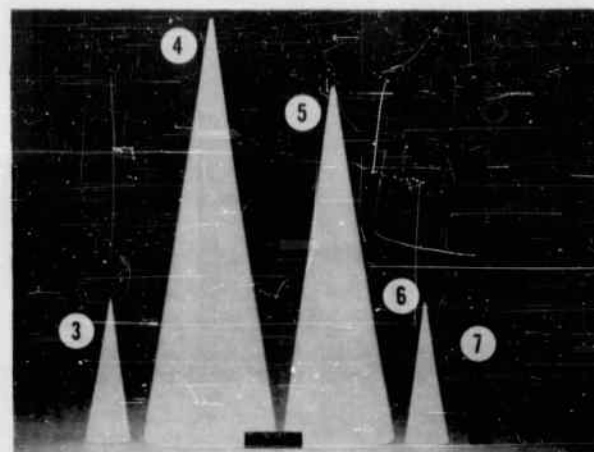


b. Tunnel Test Section

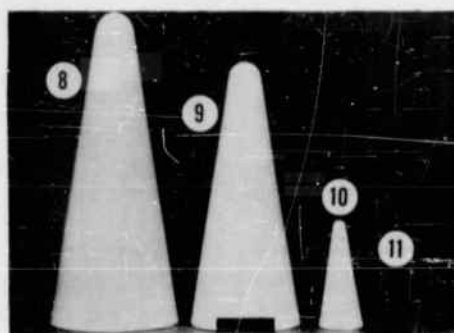
Fig. 4 The 50-Inch Mach 10 Tunnel (C)



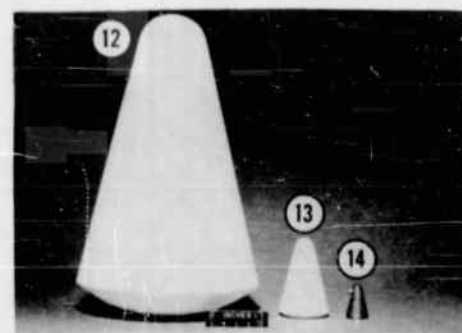
$\theta_c = 6.34 \text{ deg}$
 $\psi = 0.03 \text{ and } 0.30$



$\theta_c = 9 \text{ deg}$
 $\psi = 0 \text{ and } 0.03$

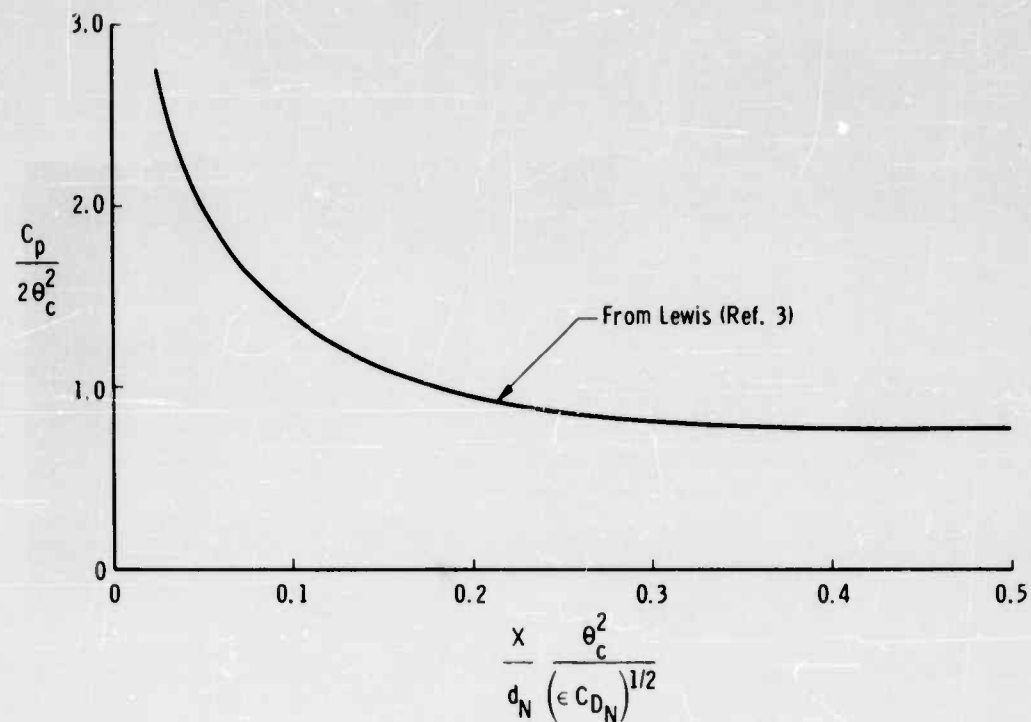
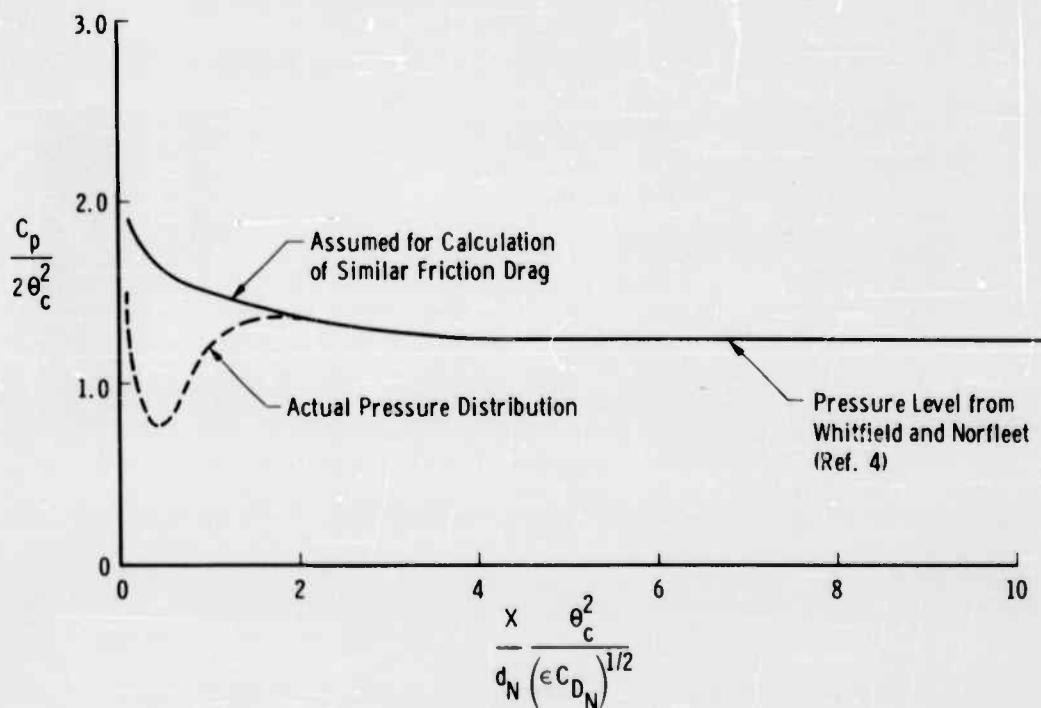


$\theta_c = 9 \text{ deg}$
 $\psi = 0.30$



$\theta_c = 13.5 \text{ deg}$
 $\psi = 0.38$

Fig. 6 Photograph of Cone Drag Models

Fig. 7 Cone Pressure Distributions for Bluntness Ratios ≥ 0.3 Fig. 8 Assumed and Actual Cone Pressure Distributions for Bluntness Ratios ≤ 0.03

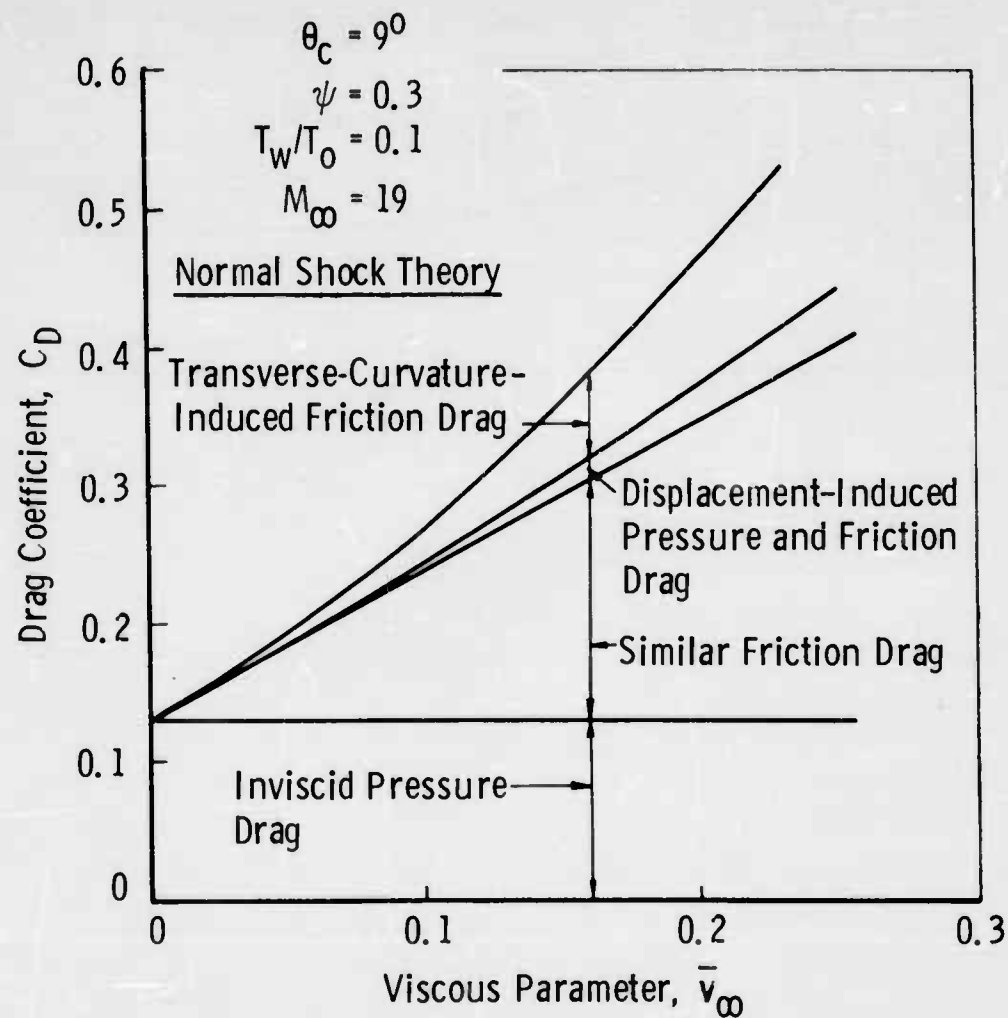


Fig. 9 Theoretical Drag Components for 9-deg Half-Vertex Angle Blunt Cone

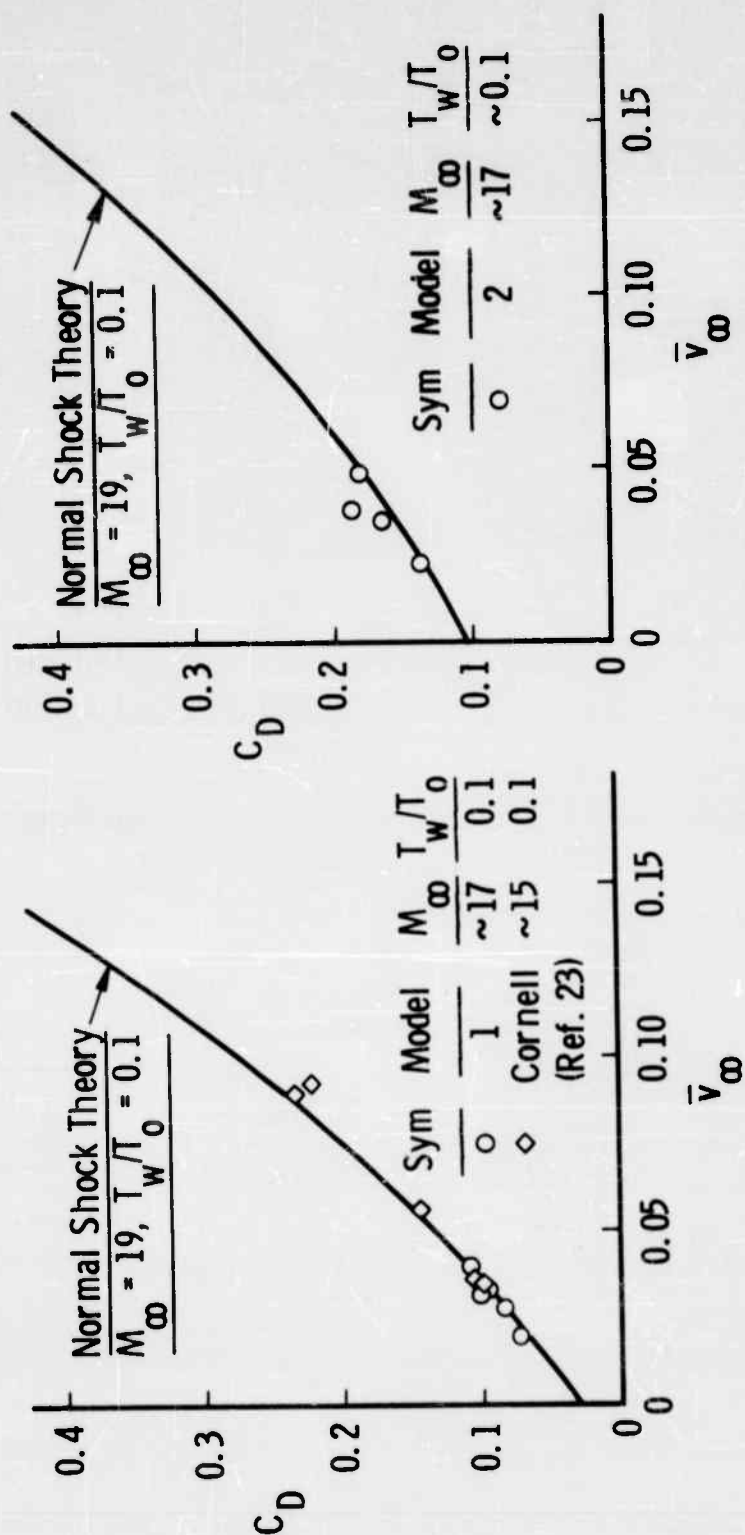
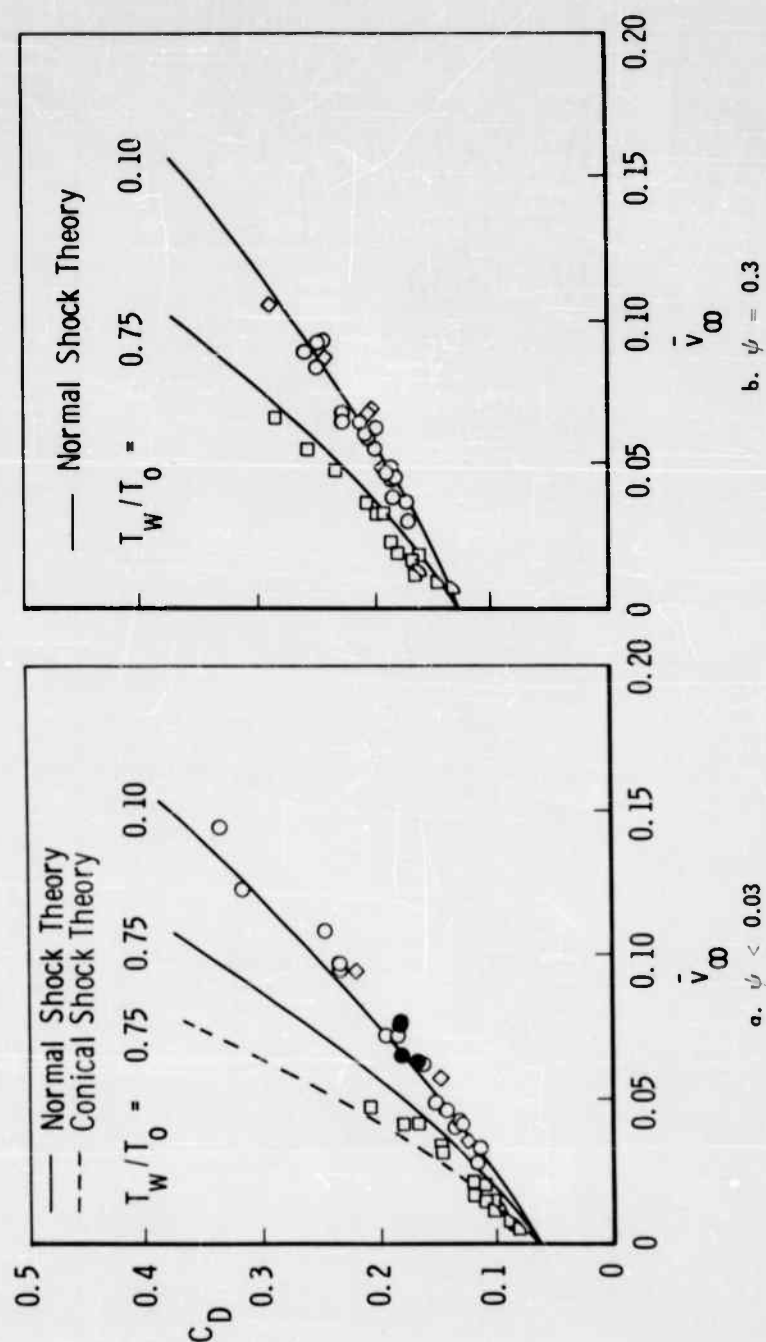
b. $\psi = 0.3$ o. $\psi = 0.03$

Fig. 10 Comparison of Theory and Experiment in Continuum Flow Regime, 6.34-deg Half-Vortex Angle Cones

Symbol	Model	M_∞	ψ	T_w/T_o
●	3	~17	~0	~0.1
○	4, 5, 6	~19	0.03	~0.1
◇	CAL (Ref. 23)	~15	0.03	~0.1
□	7a	~10	0.03	~0.75
▽	JPL (Ref. 24)	~9	~0	~0.75

Symbol	Model	M_∞	T_w/T_o
○	8, 9, 10	~19	~0.1
◇	CAL (Ref. 23)	~15	~0.1
□	11a	~10	~0.75
▽	JPL (Ref. 24)	~9	~0.75



Comparison of Theory and Experiment in Continuum Flow Regime, 9-deg Half-Vortex Angle Cones

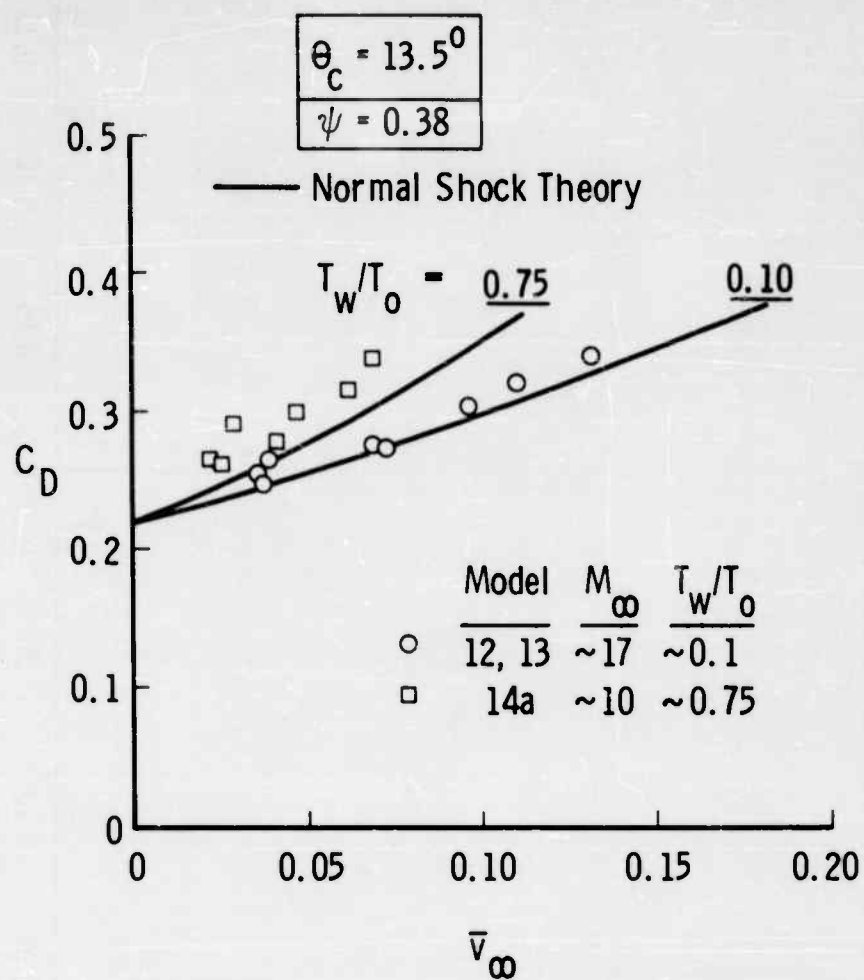


Fig. 12 Comparison of Theory and Experiment in Continuum Flow Regime,
13.5-deg Half-Vertex Angle Cone

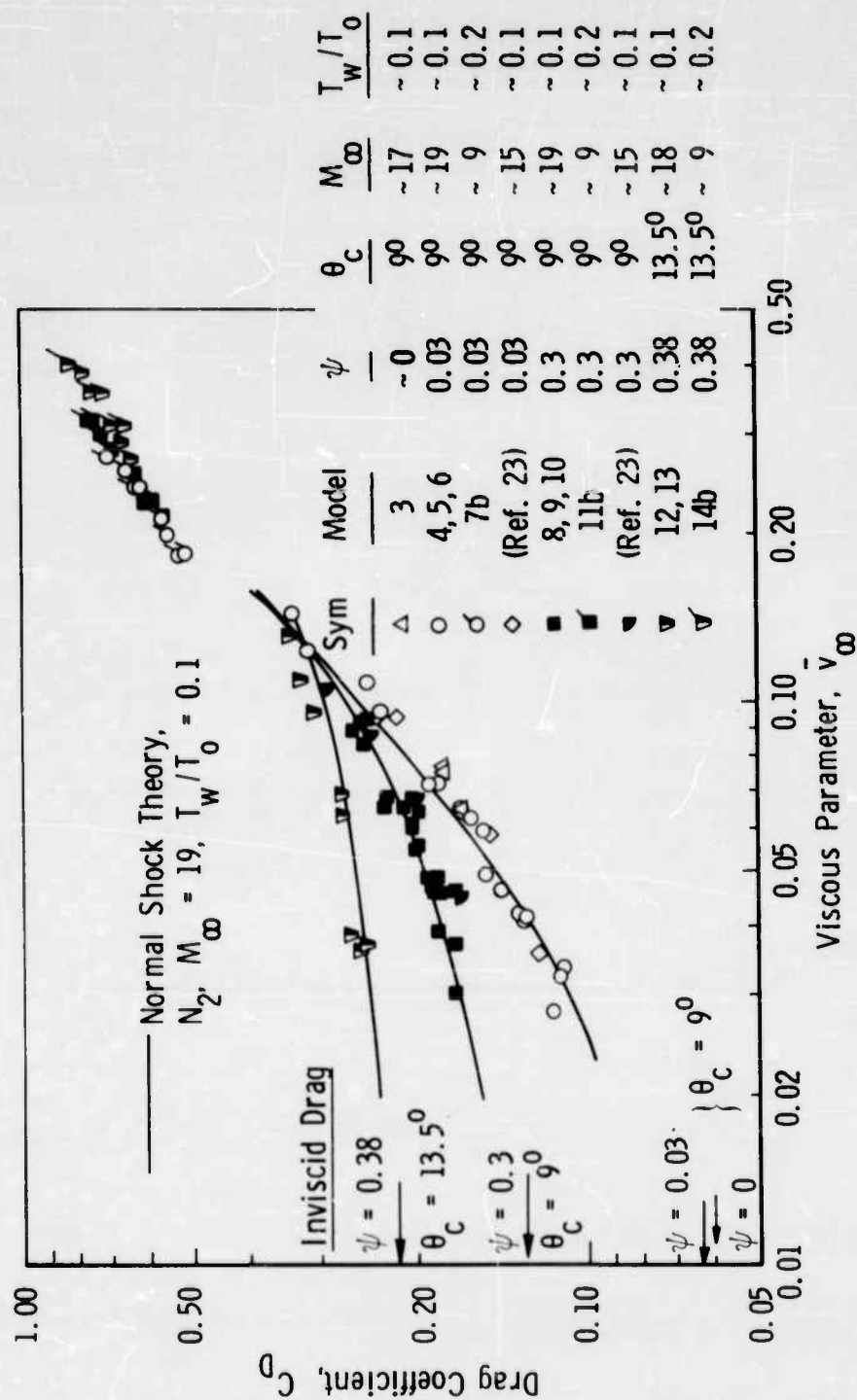


Fig. 13 Comparison of Hypersonic, Cold Wall, Viscous Drag of Blunt, Slender Cones in Continuum and Rarefied Flow Regimes

<p>Arnold Engineering Development Center Arnold Air Force Station, Tennessee Rpt. No. AEDC-TDR-63-35. VISCOUS EFFECTS ON ZERO-LIFT DRAG OF SLENDER BLUNT CONES. March 1963, 48 p. incl 2 refs., illus., tables.</p> <p>Unclassified Report</p> <p>Experimental drag data from a series of cone models are presented over a wide range of Reynolds numbers at hypersonic flow conditions. The data include Mach numbers from 9 to 22 with Reynolds numbers based on model length ranging from 600 to 500,000. Most data were obtained with test model surface temperature cold relative to the stagnation temperature; a limited amount of hot-wall data were obtained. Theoretical estimates based on existing theories are given, and the significant contributions to the zero-lift, viscous drag rise of cold-wall cones are identified as the usual "similar" or Blasius friction drag and transverse curvature effects. The theoretical estimates are shown to offer a good engineering approximation to the hypersonic viscous drag of cold-wall, blunt slender cones within the continuum flow regime.</p>	<ol style="list-style-type: none">1. Blunt bodies2. Conical bodies3. Drag4. Hypersonic characteristics <ol style="list-style-type: none">I. AFSC Program Area 806A, Project 8951, Task 895103II. Contract AF 40(600)-1000III. ARO, Inc., Arnold AF Sta., Tenn.IV. Jack D. Whitfield and B. J. GriffithV. Available from OTSVI. In ASTIA Collection	<ol style="list-style-type: none">1. Blunt bodies2. Conical bodies3. Drag4. Hypersonic characteristics <ol style="list-style-type: none">I. AFSC Program Area 806A, Project 8951, Task 895103II. Contract AF 40(600)-1000III. ARO, Inc., Arnold AF Sta., Tenn.IV. Jack D. Whitfield and B. J. GriffithV. Available from OTSVI. In ASTIA Collection
<p>Arnold Engineering Development Center Arnold Air Force Station, Tennessee Rpt. No. AEDC-TDR-63-35. VISCOUS EFFECTS ON ZERO-LIFT DRAG OF SLENDER BLUNT CONES. March 1963, 48 p. incl 2 refs., illus., tables.</p> <p>Unclassified Report</p> <p>Experimental drag data from a series of cone models are presented over a wide range of Reynolds numbers at hypersonic flow conditions. The data include Mach numbers from 9 to 22 with Reynolds numbers based on model length ranging from 600 to 500,000. Most data were obtained with test model surface temperature cold relative to the stagnation temperature; a limited amount of hot-wall data were obtained. Theoretical estimates based on existing theories are given, and the significant contributions to the zero-lift, viscous drag rise of cold-wall cones are identified as the usual "similar" or Blasius friction drag and transverse curvature effects. The theoretical estimates are shown to offer a good engineering approximation to the hypersonic viscous drag of cold-wall, blunt slender cones within the continuum flow regime.</p>	<ol style="list-style-type: none">1. Blunt bodies2. Conical bodies3. Drag4. Hypersonic characteristics <ol style="list-style-type: none">I. AFSC Program Area 806A, Project 8951, Task 895103II. Contract AF 40(600)-1000III. ARO, Inc., Arnold AF Sta., Tenn.IV. Jack D. Whitfield and B. J. GriffithV. Available from OTSVI. In ASTIA Collection	<ol style="list-style-type: none">1. Blunt bodies2. Conical bodies3. Drag4. Hypersonic characteristics <ol style="list-style-type: none">I. AFSC Program Area 806A, Project 8951, Task 895103II. Contract AF 40(600)-1000III. ARO, Inc., Arnold AF Sta., Tenn.IV. Jack D. Whitfield and B. J. GriffithV. Available from OTSVI. In ASTIA Collection

<p>Arnold Engineering Development Center Arnold Air Force Station, Tennessee Rpt. No. AEDC-TDR-83-35. VISCIOUS EFFECTS ON ZERO-LIFT DRAG OF SLENDER BLUNT CONES. March 1963, 43 p. incl 2 refs., illus., tables.</p> <p>Unclassified Report</p> <p>Experimental drag data from a series of cone models are presented over a wide range of Reynolds numbers at hypersonic flow conditions. The data include Mach numbers from 8 to 22 with Reynolds numbers based on model length ranging from 500 to 500,000. Most data were obtained with test model surface temperature cold relative to the stagnation temperature; a limited amount of hot-wall data were obtained. Theoretical estimates based on existing theories are given, and the significant contributions to the zero-lift, viscous drag rise of cold-wall cones are identified as the usual "similar" or Blasius friction drag and transverse curvature effects. The theoretical estimates are shown to offer a good engineering approximation to the hypersonic viscous drag of cold-wall, blunt slender cones within the continuum flow regime.</p>	<ol style="list-style-type: none"> 1. Blunt bodies 2. Conical bodies 3. Drag 4. Hypersonic characteristics <ol style="list-style-type: none"> I. AFSC Program Area 808A, Project 8951, Task 895103 II. ARO, Inc., Arnold AF Sta, Tenn. IV. Jack D. Whitfield and B. J. Griffith V. Available from OTS VI. In ASTIA Collection
<p>Arnold Engineering Development Center Arnold Air Force Station, Tennessee Rpt. No. AEDC-TDR-63-75. VISCIOUS EFFECTS ON ZERO-LIFT DRAG OF SLENDER BLUNT CONES. March 1963, 46 p. incl 2 refs., illus., tables.</p> <p>Unclassified Report</p> <p>Experimental drag data from a series of cone models are presented over a wide range of Reynolds numbers at hypersonic flow conditions. The data include Mach numbers from 8 to 22 with Reynolds numbers based on model length ranging from 500 to 500,000. Most data were obtained with test model surface temperature cold relative to the stagnation temperature; a limited amount of hot-wall data were obtained. Theoretical estimates based on existing theories are given, and the significant contributions to the zero-lift, viscous drag rise of cold-wall cones are identified as the usual "similar" or Blasius friction drag and transverse curvature effects. The theoretical estimates are shown to offer a good engineering approximation to the hypersonic viscous drag of cold-wall, blunt slender cones within the continuum flow regime.</p>	<ol style="list-style-type: none"> 1. Blunt bodies 2. Conical bodies 3. Drag 4. Hypersonic characteristics <ol style="list-style-type: none"> I. AFSC Program Area 808A, Project 8951, Task 895103 II. ARO, Inc., Arnold AF Sta, Tenn. IV. Jack D. Whitfield and B. J. Griffith V. Available from OTS VI. In ASTIA Collection

<p>Arnold Engineering Development Center Arnold Air Force Station, Tennessee Rpt. No. AEDC-TDR-63-35. VISCOUS EFFECTS ON ZERO-LIFT DRAG OF SLENDER BLUNT CONES. March 1963, 48 p. incl 2 refs., illus., tables.</p> <p>Unclassified Report</p> <p>Experimental drag data from a series of cone models are presented over a wide range of Reynolds numbers at hypersonic flow conditions. The data include Mach numbers from 9 to 22 with Reynolds numbers based on model length ranging from 600 to 500,000. Most data were obtained with test model surface temperature cold relative to the stagnation temperature; a limited amount of hot-wall data were obtained. Theoretical estimates based on existing theories are given, and the significant contributions to the zero-lift, viscous drag rise of cold-wall cones are identified as the usual "similar" or Blasius friction drag and transverse curvature effects. The theoretical estimates are shown to offer a good engineering approximation to the hypersonic viscous drag of cold-wall, blunt slender cones within the continuum flow regime.</p>	<ol style="list-style-type: none"> 1. Blunt bodies 2. Conical bodies 3. Drag 4. Hypersonic characteristics I. AFSC Program Area 806A, Project 8951, Task 895103 II. Contract AF 40(600)-1000 III. ARO, Inc., Arnold AF Sta, Tenn. IV. Jack D. Whitfield and B. J. Griffith V. Available from OTS VI. In ASTIA Collection
<p>Arnold Engineering Development Center Arnold Air Force Station, Tennessee Rpt. No. AEDC-TDR-33-35. VISCOUS EFFECTS ON ZERO-LIFT DRAG OF SLENDER BLUNT CONES. March 1963, 48 p. incl 2 refs., illus., tables.</p> <p>Unclassified Report</p> <p>Experimental drag data from a series of cone models are presented over a wide range of Reynolds numbers at hypersonic flow conditions. The data include Mach numbers from 9 to 22 with Reynolds numbers based on model length ranging from 600 to 500,000. Most data were obtained with test model surface temperature cold relative to the stagnation temperature; a limited amount of hot-wall data were obtained. Theoretical estimates based on existing theories are given, and the significant contributions to the zero-lift, viscous drag rise of cold-wall cones are identified as the usual "similar" or Blasius friction drag and transverse curvature effects. The theoretical estimates are shown to offer a good engineering approximation to the hypersonic viscous drag of cold-wall, blunt slender cones within the continuum flow regime.</p>	<ol style="list-style-type: none"> 1. Blunt bodies 2. Conical bodies 3. Drag 4. Hypersonic characteristics I. AFSC Program Area 806A, Project 8951, Task 895103 II. Contract AF 40(600)-1000 III. ARO, Inc., Arnold AF Sta, Tenn. IV. Jack D. Whitfield and B. J. Griffith V. Available from OTS VI. In ASTIA Collection

<p>Arnold Engineering Development Center Arnold Air Force Station, Tennessee Rpt. No. AEDC-TDR-63-35. VISCOUS EFFECTS ON ZERO-LIFT DRAG OF SLENDER BLUNT CONES. March 1963, 48 p. incl 2 refs., illus., tables.</p> <p>Unclassified Report</p> <p>Experimental drag data from a series of cone models are presented over a wide range of Reynolds numbers at hypersonic flow conditions. The data include Mach numbers from 9 to 22 with Reynolds numbers based on model length ranging from 600 to 500,000. Most data were obtained with test model surface temperature cold relative to the stagnation temperature; a limited amount of hot-wall data were obtained. Theoretical estimates based on existing theories are given, and the significant contributions to the zero-lift, viscous drag rise of cold-wall cones are identified as the usual "similar" or Blasius friction drag and transverse curvature effects. The theoretical estimates are shown to offer a good engineering approximation to the hypersonic viscous drag of cold-wall, blunt slender cones within the continuum flow regime.</p>	<p>1. Blunt bodies 2. Conical bodies 3. Drag 4. Hypersonic characteristics I. AFSC Program Area 806A, Project 8951, Task 895103 II. Contract AF 40(600)-1000 III. ARO, Inc., Arnold AF Sta, Tenn. IV. Jack D. Whitfield and B. J. Griffith V. Available from OTS VI. In ASTIA Collection</p>	
<p>Arnold Engineering Development Center Arnold Air Force Station, Tennessee Rpt. No. AEDC-TDR-63-35. VISCOUS EFFECTS ON ZERO-LIFT DRAG OF SLENDER BLUNT CONES. March 1963, 48 p. incl 2 refs., illus., tables.</p> <p>Unclassified Report</p> <p>Experimental drag data from a series of cone models are presented over a wide range of Reynolds numbers at hypersonic flow conditions. The data include Mach numbers from 9 to 22 with Reynolds numbers based on model length ranging from 600 to 500,000. Most data were obtained with test model surface temperature cold relative to the stagnation temperature; a limited amount of hot-wall data were obtained. Theoretical estimates based on existing theories are given, and the significant contributions to the zero-lift, viscous drag rise of cold-wall cones are identified as the usual "similar" or Blasius friction drag and transverse curvature effects. The theoretical estimates are shown to offer a good engineering approximation to the hypersonic viscous drag of cold-wall, blunt slender cones within the continuum flow regime.</p>	<p>1. Blunt bodies 2. Conical bodies 3. Drag 4. Hypersonic characteristics I. AFSC Program Area 806A, Project 8951, Task 895103 II. Contract AF 40(600)-1000 III. ARO, Inc., Arnold AF Sta, Tenn. IV. Jack D. Whitfield and B. J. Griffith V. Available from OTS VI. In ASTIA Collection</p>	

<p>Arnold Engineering Development Center Arnold Air Force Station, Tennessee Rpt. No. AEDC-TDR-63-35. VISCOUS EFFECTS ON ZERO-LIFT DRAG OF SLENDER BLUNT CONES. March 1963. 48 p. incl 2 refs., illus., tables.</p> <p>Unclassified Report</p> <p>Experimental drag data from a series of cone models are presented over a wide range of Reynolds numbers at hypersonic flow conditions. The data include Mach numbers from 9 to 22 with Reynolds numbers based on model length ranging from 600 to 500,000. Most data were obtained with test model surface temperature cold relative to the stagnation temperature; a limited amount of hot-wall data were obtained. Theoretical estimates based on existing theories are given, and the significant contributions to the zero-lift, viscous drag rise of cold-wall cones are identified as the usual "similar" or Blasius friction drag and transverse curvature effects. The theoretical estimates are shown to offer a good engineering approximation to the hypersonic viscous drag of cold-wall, blunt slender cones within the continuum flow regime.</p>	<ol style="list-style-type: none"> 1. Blunt bodies 2. Conical bodies 3. Drag 4. Hypersonic characteristics <ol style="list-style-type: none"> I. AFSC Program Area 806A, Project 8951, Task 895103 II. ARO, Inc., Arnold AF Sta., Tenn. III. Jack D. Whitfield and B. J. Griffith IV. Available from OTS V. In ASTIA Collection
<p>Arnold Engineering Development Center Arnold Air Force Station, Tennessee Rpt. No. AEDC-TDR-63-35. VISCOUS EFFECTS ON ZERO-LIFT DRAG OF SLENDER BLUNT CONES. March 1963. 48 p. incl 2 refs., illus., tables.</p> <p>Unclassified Report</p> <p>Experimental drag data from a series of cone models are presented over a wide range of Reynolds numbers at hypersonic flow conditions. The data include Mach numbers from 9 to 22 with Reynolds numbers based on model length ranging from 600 to 500,000. Most data were obtained with test model surface temperature cold relative to the stagnation temperature; a limited amount of hot-wall data were obtained. Theoretical estimates based on existing theories are given, and the significant contributions to the zero-lift, viscous drag rise of cold-wall cones are identified as the usual "similar" or Blasius friction drag and transverse curvature effects. The theoretical estimates are shown to offer a good engineering approximation to the hypersonic viscous drag of cold-wall, blunt slender cones within the continuum flow regime.</p>	<ol style="list-style-type: none"> 1. Blunt bodies 2. Conical bodies 3. Drag 4. Hypersonic characteristics <ol style="list-style-type: none"> I. AFSC Program Area 806A, Project 8951, Task 895103 II. ARO, Inc., Arnold AF Sta., Tenn. III. Jack D. Whitfield and B. J. Griffith IV. Available from OTS V. In ASTIA Collection
<p>Arnold Engineering Development Center Arnold Air Force Station, Tennessee Rpt. No. AEDC-TDR-63-35. VISCOUS EFFECTS ON ZERO-LIFT DRAG OF SLENDER BLUNT CONES. March 1963. 48 p. incl 2 refs., illus., tables.</p> <p>Unclassified Report</p> <p>Experimental drag data from a series of cone models are presented over a wide range of Reynolds numbers at hypersonic flow conditions. The data include Mach numbers from 9 to 22 with Reynolds numbers based on model length ranging from 600 to 500,000. Most data were obtained with test model surface temperature cold relative to the stagnation temperature; a limited amount of hot-wall data were obtained. Theoretical estimates based on existing theories are given, and the significant contributions to the zero-lift, viscous drag rise of cold-wall cones are identified as the usual "similar" or Blasius friction drag and transverse curvature effects. The theoretical estimates are shown to offer a good engineering approximation to the hypersonic viscous drag of cold-wall, blunt slender cones within the continuum flow regime.</p>	<ol style="list-style-type: none"> 1. Blunt bodies 2. Conical bodies 3. Drag 4. Hypersonic characteristics <ol style="list-style-type: none"> I. AFSC Program Area 806A, Project 8951, Task 895103 II. ARO, Inc., Arnold AF Sta., Tenn. III. Jack D. Whitfield and B. J. Griffith IV. Available from OTS V. In ASTIA Collection

<p>Arnold Engineering Development Center Arnold Air Force Station, Tennessee Rpt. No. AEDC-TDR-63-35. VISCOUS EFFECTS ON ZERO-LIFT DRAG OF SLENDER BLUNT CONES. March 1963, 48 p. incl 2 refs., illus., tables.</p> <p>Unclassified Report</p> <p>Experimental drag data from a series of cone models are presented over a wide range of Reynolds numbers at hypersonic flow conditions. The data include Mach numbers from 9 to 22 with Reynolds numbers based on model length ranging from 600 to 500,000. Most data were obtained with test model surface temperature cold relative to the stagnation temperature; a limited amount of hot-wall data were obtained. Theoretical estimates based on existing theories are given, and the significant contributions to the zero-lift, viscous drag rise of cold-wall cones are identified as the usual "similar" or Blasius friction drag and transverse curvature effects. The theoretical estimates are shown to offer a good engineering approximation to the hypersonic viscous drag of cold-wall, blunt slender cones within the continuum flow regime.</p>	<ol style="list-style-type: none"> 1. Blunt bodies 2. Conical bodies 3. Drag 4. Hypersonic characteristics <ol style="list-style-type: none"> I. AFSC Program Area 806A, Project 8951, Task 895103 II. Contract AF 40(600)-1000 III. ARO, Inc., Arnold AF Sta, Tenn. IV. Jack D. Whitfield and B. J. Griffith V. Available from OTS VI. In ASTIA Collection
<p>Arnold Engineering Development Center Arnold Air Force Station, Tennessee Rpt. No. AEDC-TDR-63-35. VISCOUS EFFECTS ON ZERO-LIFT DRAG OF SLENDER BLUNT CONES. March 1963, 48 p. incl 2 refs., illus., tables.</p> <p>Unclassified Report</p> <p>Experimental drag data from a series of cone models are presented over a wide range of Reynolds numbers at hypersonic flow conditions. The data include Mach numbers from 9 to 22 with Reynolds numbers based on model length ranging from 600 to 500,000. Most data were obtained with test model surface temperature cold relative to the stagnation temperature; a limited amount of hot-wall data were obtained. Theoretical estimates based on existing theories are given, and the significant contributions to the zero-lift, viscous drag rise of cold-wall cones are identified as the usual "similar" or Blasius friction drag and transverse curvature effects. The theoretical estimates are shown to offer a good engineering approximation to the hypersonic viscous drag of cold-wall, blunt slender cones within the continuum flow regime.</p>	<ol style="list-style-type: none"> 1. Blunt bodies 2. Conical bodies 3. Drag 4. Hypersonic characteristics <ol style="list-style-type: none"> I. AFSC Program Area 806A, Project 8951, Task 895103 II. Contract AF 40(600)-1000 III. ARO, Inc., Arnold AF Sta, Tenn. IV. Jack D. Whitfield and B. J. Griffith V. Available from OTS VI. In ASTIA Collection
<p>Arnold Engineering Development Center Arnold Air Force Station, Tennessee Rpt. No. AEDC-TDR-63-35. VISCOUS EFFECTS ON ZERO-LIFT DRAG OF SLENDER BLUNT CONES. March 1963, 48 p. incl 2 refs., illus., tables.</p> <p>Unclassified Report</p> <p>Experimental drag data from a series of cone models are presented over a wide range of Reynolds numbers at hypersonic flow conditions. The data include Mach numbers from 9 to 22 with Reynolds numbers based on model length ranging from 600 to 500,000. Most data were obtained with test model surface temperature cold relative to the stagnation temperature; a limited amount of hot-wall data were obtained. Theoretical estimates based on existing theories are given, and the significant contributions to the zero-lift, viscous drag rise of cold-wall cones are identified as the usual "similar" or Blasius friction drag and transverse curvature effects. The theoretical estimates are shown to offer a good engineering approximation to the hypersonic viscous drag of cold-wall, blunt slender cones within the continuum flow regime.</p>	<ol style="list-style-type: none"> 1. Blunt bodies 2. Conical bodies 3. Drag 4. Hypersonic characteristics <ol style="list-style-type: none"> I. AFSC Program Area 806A, Project 8951, Task 895103 II. Contract AF 40(600)-1000 III. ARO, Inc., Arnold AF Sta, Tenn. IV. Jack D. Whitfield and B. J. Griffith V. Available from OTS VI. In ASTIA Collection